Interplay between PLEKHG3-regulated actin dynamics and lysosomal trafficking in cell motility

Rainer Ettelt[1,2], Georg Vucak[1,2], Sebastian Didusch[1,2], Biljana Riemelmoser[1], Karin Ehrenreiter[1], Markus Hartl[3], Lukas A. Huber[4] and Manuela Baccarini[1]

[1] University of Vienna, Center for Molecular Biology, Department of Microbiology, Immunobiology and Genetics, Max Perutz Labs, Vienna Biocenter Campus (VBC) Dr.-Bohr-Gasse 9, 1030, Vienna, Austria; [2] Vienna BioCenter PhD Program, Doctoral School of the University of Vienna and Medical University of Vienna, Vienna, Austria; [3] Department of Biochemistry and Cell Biology, Max Perutz Labs, University of Vienna, Vienna BioCenter, Vienna, Austria; [4] Institute of Cell Biology, Biocenter, Medical University of Innsbruck, Innsbruck, Austria

Correspondence to Manuela Baccarini: manuela.baccarini@univie.ac.at

Abstract

Lysosomes are highly dynamic organelles that regulate metabolic signaling pathways by recruiting cytosolic molecules to protein platforms on the lysosomal membrane. We performed a proximity-dependent labeling screen to identify novel proteins recruited to the LAMTOR complex, which regulates lysosome positioning and key signaling pathways such as mTORC1, AMPK, and MEK/ERK. We identified a network of proteins involved in actin remodelling, including Pleckstrin homology domain-containing family G member 3 (PLEKHG3), an actin-binding Rho guanine nucleotide exchange factor enriched in protrusions. We show that GFP-PLEKHG3 accumulates in focal adhesion sites, where it colocalizes with peripheral lysosomes. Peripheral accumulation of lysosomes concentrates PLEKHG3 below the plasma membrane, inhibits protrusion formation and limits cell motility. Thus, subcellular positioning of lysosomes impacts PLEKHG3 subcellular localization and the cell's protrusion activity, shape, and motility. The results shed new light

on the interplay between lysosomes and actin dynamics and provides insights into the mechanisms controlling cellular processes such as shape regulation and motility of the plasma membrane.

Introduction

Lysosomes are acidic organelles that degrade proteins, nucleic acids and other macromolecules to replenish the cell's pool of metabolic building blocks. Lysosomes are highly dynamic, in terms of size and location within the cell, and are capable of making contact and fusing with other organelles such as the ER. The lysosomes' limiting membrane contains a wide repertoire of resident transmembrane and membrane-associated proteins and protein complexes that dynamically recruit cytosolic proteins involved in signaling and metabolic processes (Ballabio and Bonifacino, 2020).

One of these resident protein complexes is the late endosomal/lysosomal adaptor and MAPK and mTOR activator (LAMTOR) complex, also named Ragulator, based on its ability to recruit the small Rag GTPases essential for mTORC1 regulation. The pentameric LAMTOR complex consist of two heterodimers LAMTOR2 (p14) /LAMTOR3 (MP1) and LAMTOR4 (C11orf59)/LAMTOR5 (HBXIP) held together by the belt-like, myristoylated LAMTOR1 (p18) subunit that anchors them to the lysosomal surface (de Araujo et al., 2017). The LAMTOR complex integrates mTORC1 activation (Sancak et al., 2010), MEK/ERK signaling (Teis et al., 2002), AMPK signaling (Zhang et al., 2014), lysosomal size regulation (Vogel et al., 2015; de Araujo et al., 2020) and lysosome positioning (Filipek et al., 2017; Pu et al., 2017).

Lysosome positioning affects the organelle's physico-chemical properties such as its luminal pH, content and activity of digestive enzymes (Johnson et al., 2016; Kumar et al., 2022). In terms of signalling, increased mTORC1 activation has been correlated with accumulation of lysosomes in the periphery (Hong et al., 2017; Korolchuk et al., 2011) and more specifically with the association of lysosomes with focal adhesion sites (FA) (Rabanal-Ruiz et al., 2021). Peripheral lysosomes have also been implicated in fusion processes occurring at the plasma

membrane (PM), such as antigen presentation, membrane repair and cellular clearance by lysosomal exocytosis, through which they release intracellular content into the extracellular space (Rodríguez et al., 1997; Andrews, 2000; Medina et al., 2011; Buratta et al., 2020). To reach the PM, lysosomes have to transition from the microtubule tracks, on which they move through the cell, to the cortical actin mesh (Cabukusta and Neefjes, 2018; Pu et al., 2016). It has been shown that lysosomes use myosin motor proteins to move along actin filaments in a manner similar to their kinesin- or dynein-directed movement on microtubule tracks (Caviston et al., 2011; Cordonnier et al., 2001). The interaction with the dense cortical actin network causes transient retention of lysosomes in the periphery of the cell (Caviston et al., 2011; Encarnação et al., 2016).

In order to obtain a complete picture of the proteins associated with lysosomes, numerous approaches have been pursued (Bagshaw et al., 2003, 2005; Schröder et al., 2007; della Valle et al., 2011; Chapel et al., 2013), but the identification of transient interactors or vicinal proteins has remained a challenge. Recently, utilization of proximity-dependent labeling screens (Go et al., 2021; Liao et al., 2019; Liu et al., 2018; Tan and Finkel, 2022) has led to the identification of previously unknown lysosomal and lysosome-associated proteins. However, these approaches were either limited by the ligase used due to long labeling times (BirA*), the requirement of cytotoxic reagents (APEX) or by the baits used. In this study we focus on finding new cytoplasmic proteins recruited to the lysosomal surface using LAMTOR3 as a bait in a TurboID proximity-dependent labelling screen. One of the main components of the LAMTOR3 (L3) proxysome was PLEKHG3, an understudied protein that contributes to cortical actin remodeling by binding selectively to newly polymerized actin at the cell's leading edge. PLEKHG3 induces a positive feedback on actin polymerization by acting as a GEF for Rac1 and CDC42 downstream of PI3K promotes Rac-mediated membrane ruffling downstream of

RHOG (Nguyen et al., 2016; Bagci et al., 2020). We demonstrate that PLEKHG3 colocalizes with lysosomes at focal adhesion and protrusion sites, and that the localization and function of this protein, as well as cell motility – which we define as the sum of membrane remodeling processes involved in migration – depend on lysosomal dynamics.

Results

Proximity-dependent labelling reveals an interaction between L3 and the actin remodelling network

The resident pentameric lysosomal LAMTOR/Ragulator complex has been identified as a signaling hub for growth factor and metabolic signaling.

Towards the unbiased identification of novel proteins that can be recruited to the limiting membrane of lysosomes, we performed a mass spectrometry (MS)-coupled proximity-dependent labeling screen (Figure 1A) using the LAMTOR component LAMTOR3 (L3) as bait. Lentiviral constructs containing TurboID-V5 tags fused to the C terminus of L3 (L3-T-V5) or to GFP-NES (nuclear export signal; GFP-T-V5, specificity control) under the control of a doxycycline-dependent promoter were used to generate stable HEK293T cell lines that expressed the baits at similar levels (Figure S1A-B). Immunofluorescence confirmed the predominantly lysosomal localization of the L3-T-V5 bait and its colocalization with the lysosomal-associated membrane protein 1 (LAMP1) (Figure S1C). Analysis of prey proteins specifically biotinylated by the L3 bait yielded an interaction network of known L3 binding partners including the other LAMTOR subunits, parts of the BORC complex, the neutral amino acid transporter SLC38A9 as well as several proteins involved in regulation of mTORC1 activity, in addition to several novel proteins (Figure S1D).

We next performed an ortholog screen using V5-TurboID fused to the N terminus of L3 (V5-T-L3) and V5- TurboID fused to NES as a cytosolic specificity control (V5-CYTO; see Figure S1E). Considering the predominantly lysosomal localization of the L3 baits observed in Figure S1C and F, we also generated a signpost for lysosomal biotinylation (V5-LYSO) consisting of V5-TurboID fused to the lysosomal transmembrane protein TMEM192 (Figure S1E). Using the doxycycline-inducible Flp-In™ T-REx™ system (Invitrogen™) we achieved close to

endogenous, homogenous expression of the bait proteins (Figure S1G). We then grew these cells in full medium (FM) or exposed them to starvation (EBSS, growth factor + amino acid starvation) and restimulation (EBSS + 10 minutes FM), to discover interactions induced by these conditions (Figure S1H). This screen confirmed many of the interactors identified in the previous one, including the LAMTOR subunits (LAMTOR1-5), the Rag GTPases and RAPTOR as a representative subunit of the mTORC1 complex, parts of the BORC complex, as well as a subunit of the vATPase (Figure S1I). Indeed, the majority of the hits (~64% for V5-T-L3 and ~67% for L3-T-V5) were identified in both screens, irrespective of the differences in the experimental systems used (specific vs random integration, homogenous vs heterogenous expression; cell line specific differences; ligase positioning in the complex; cytosolic control baits), strengthening confidence in the robustness and reliability of the screens (Figure 1B). Some hits, however, were specific to one of the baits, most prominently GATOR1, which was labeled by L3-T-V5 but not by V5-T-L3 bait. In turn, only V5-T-L3 was able to label the GATOR2 complex (Figure 1B-C) as well as several lysosomal proteins, indirect or transient interactors not identified in previous studies (Figure 1D) (reviewed in Colaço and Jäättelä, 2017; Rogala et al., 2019; Egri et al., 2022). Finally, L3-T-V5 labeled subunits of the BORC missed by V5-T-L3, yielding a more complete picture of L3's interactors (Figure 1D). Somewhat surprisingly, the L3 proxisome was very similar in fed, starved, and restimulated cells (Figure S1J-K).

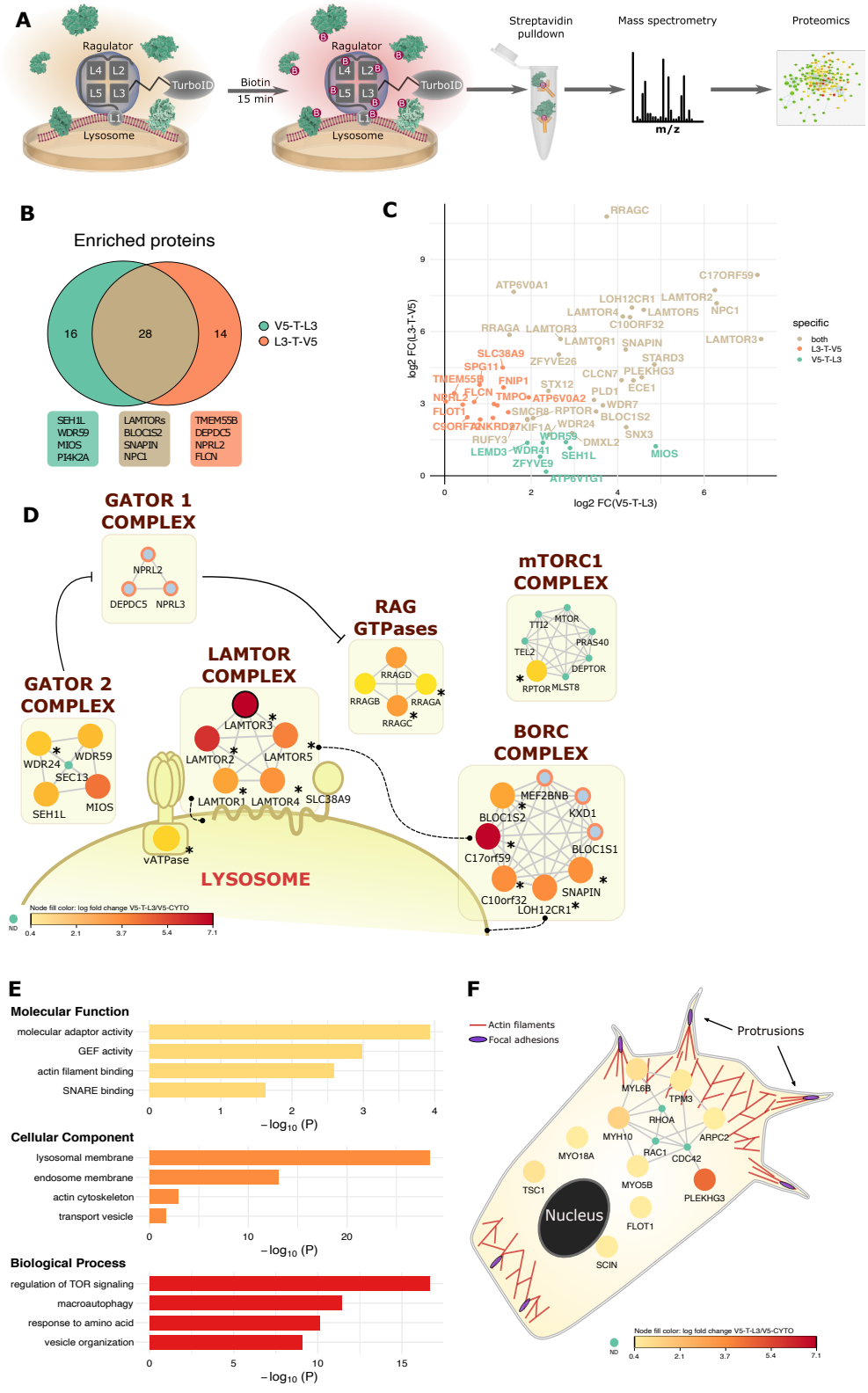

Figure 1: Bioinformatics analysis of L3-TurboID PDL screen. A) Workflow of TurboID screens. Cells were treated with biotin for 10-15 minutes prior to lysis and isolation of biotinylated proteins and mass spectrometry. **B)** Venn-diagram of complementary TurboID screens using C-terminally (L3-T-V5) and N-terminally (V5-T-L3) tagged L3. Shown are hits significantly enriched in L3 over the respective cytosolic controls and in V5-LYSO over V5-CYTO (log2 FC ≥ 1.49 and adj. p-value ≤ 0.05). **C)** Fold change plot combining the results of both screens. **D)** Network representation of the complementary L3-TurboID datasets. Depicted proteins are regulators of mTORC1 signaling and well-described interactors of the Ragulator complex. For the hits detected by V5-T-L3

(outlined in black), color coding indicates fold change over V5-CYTO. Proteins detected only by L3-T-V5 are shown as light blue nodes circled in orange. Asterisks mark proteins detected in both screens. Proteins that are part of the networks identified in our screen but not detected by either bait are shown as green dots. Broken lines indicate protein-protein or protein-membrane interactions. **E)** Gene ontology overrepresentation analysis (ORA) of proteins significantly enriched in V5-T-L3 over V5-CYTO. GEF, Guanine nucleotide exchange factor. **F)** network and functional representation of V5-T-L3 hits enriched in the GO-terms actin filament binding and actin cytoskeleton, plus manually curated hits. Color coding indicates enrichment over V5-CYTO-TurboID. Actin filaments are shown in red and FAs in purple. Proteins not detected by V5-T-L3 are shown as green dots.

Comparison of the proteins biotinylated by V5-T-L3 and by the V5-LYSO signpost, respectively, revealed a strong overlap, particularly in proteins found in the proximity of the lysosomal membrane. However, a number of hits were specifically biotinylated by V5-T-L3 and could not be detected among the V5-LYSO preys or the V5-CYTO control preys (see Figure S1K). Overrepresentation analysis (ORA) of the proteins detected by the V5-T-L3 bait returned "molecular adaptor activity" as the main molecular function, and lysosomal membrane/ endosome membrane as top scored cellular component. mTORC1 and autophagy regulation were at the top of the biological processes (Figure 1E). While these molecular functional groups were not unexpected, we also identified a specific subset of proteins involved in actin remodelling, including the GO-terms "GEF activity and actin filament binding" and "localization to the actin cytoskeleton" (Figure 1E-F). Most of these hits were significantly enriched although not very abundant (Supplementary Table 1), but one protein in this network, PLEKHG3, ranked among the top hits in both screens (Figure 1C and F). PLEKHG3 is an understudied protein consisting of a Dbl-homology (DH) domain to execute its RhoGEF activity, a Plekstrin homology (PH) domain important for its binding to phosphoinositides at the PM, and an actin binding domain (ABD). PLEKHG3 has been described to colocalize with actin filaments, more specifically accumulating at sites of membrane remodelling such as the leading or the trailing edges. Its identification in our screens opened the more general the

question of a specific role of lysosomes in actin remodeling, possibly mediated by L3. (Nguyen et al., 2016; Bagci et al., 2020).

PLEKHG3 is a proximal protein of L3 that colocalizes with peripheral lysosomes at cell protrusions

The above results made PLEKHG3 a promising candidate to focus on. To verify the specificity of available PLEKHG3 reagents, we tested an antibody described as applicable for immunoblotting and immunofluorescence. Immunoblotting displayed multiple bands with molecular weights (MW) whose intensity dropped significantly upon siRNA-based knockdown of PLEKHG3 both, in HeLa and in HEK293T cells (Figure S2A-B). Thus, the antibody recognized PLEKHG3, although as previously described (Bagci et al., 2020), the molecular weight of the protein in SDS-PAGE is much higher than the 134 kDa calculated from the amino acid sequence of the protein (Figure S2B).

Immunofluorescence analysis of the same PLEKHG3 antibody revealed colocalization of endogenous PLEKHG3 with Phalloidin in HEK293T cells which was selectively reduced at the plasma membrane upon PLEKHG3 KD (Figure S2C). Confirming the high molecular weight of endogenous PLEKHG3 on the Western blot (Figure S2B), expression of exogenous GFP-PLEKHG3 also revealed a much higher molecular weight of this protein on SDS-PAGE than the predicted 164 kDa (Figure S2D). Furthermore, colocalization was shown with the exogenous GFP-PLEKHG3 signal, and a significant drop in both the PLEKHG3 and the GFP signal upon PLEKHG3 knockdown (Figure S2E-F). Together, the experiments validated the PLEKHG3 reagents.

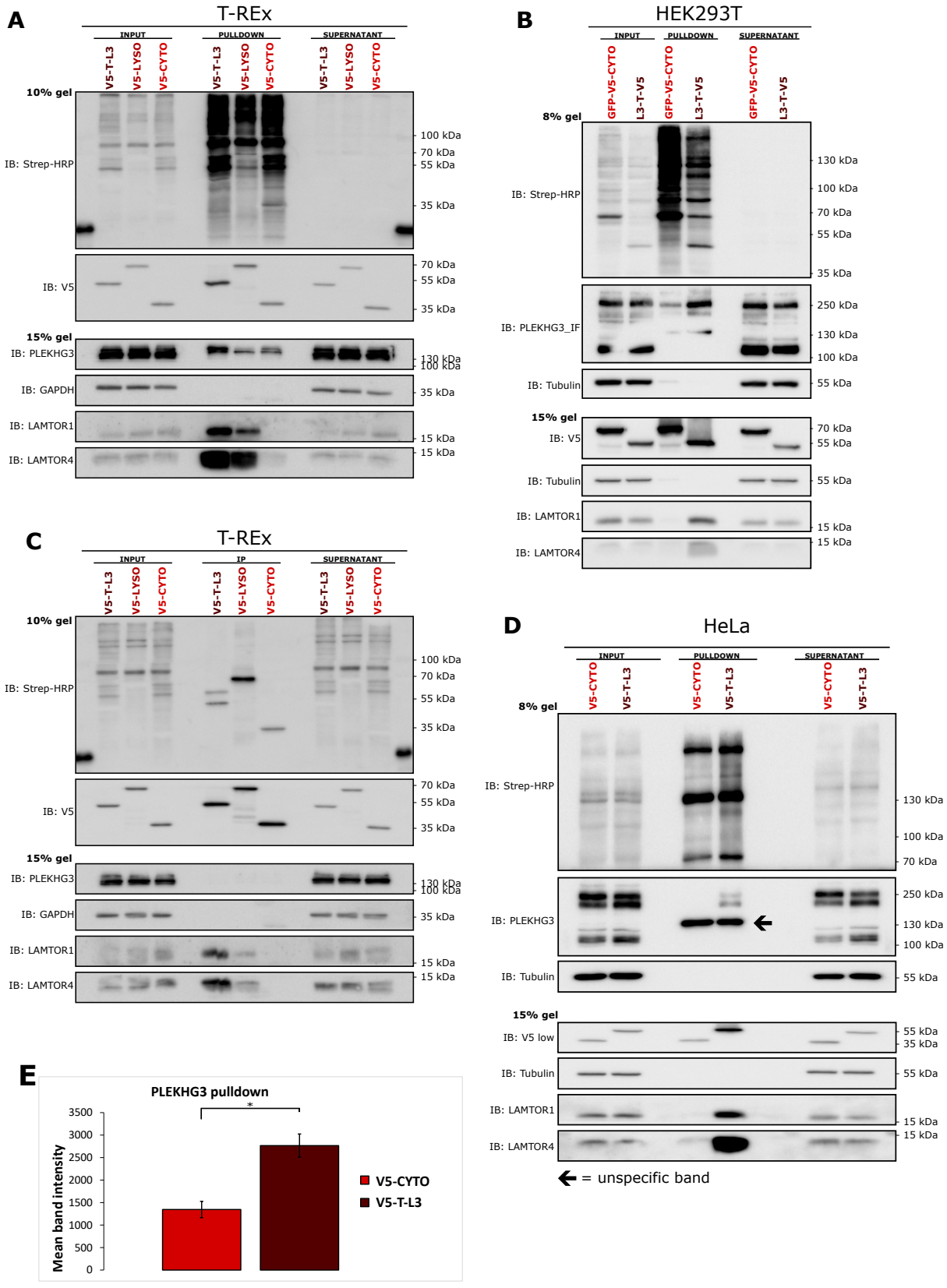

Figure 2: PLEKHG3 is a proximal protein or transient interactor of L3. A-B) Biotinylated proteins were isolated either from HEK293T cells stably expressing L3-T-V5 or GFP-V5-CYTO (left) or from T-REx cells stably expressing V5-T-L3, the V5-LYSO signpost, or the V5-CYTO control (right) and subjected to SDS-PAGE. L1 and L4 serve as positive controls for direct interaction partners. **C)** V5 pulldown from T-REx cells expressing V5-T-L3, the V5-LYSO signpost, or the V5-CYTO control were subjected to SDS-PAGE and immunoblotted for an PLEKHG3 antibody to

detect interaction. **D)** Representative immunoblot of proteins biotinylated by V5-T-L3 and V5-CYTO. GAPDH serves as a loading control (input and supernatant) and as a specificity control for the pulldowns. The band marked by an arrow is only present in the streptavidin pulldowns but not in the input or supernatant and is therefore considered unspecific. **E)** Quantification of PLEKHG3 bands from immunoblots similar to the one shown in C. Error bars = SEM, n=3. * = p values according to student's t-test.

To validate the results obtained by MS, we isolated biotinylated proteins from T-REx and HEK293T cells and found PLEKHG3 specifically enriched in streptavidin pulldowns from cells expressing the L3 baits (L3-T-V5 or V5-T-L3) compared to the pulldowns from cells expressing the respective controls (Figure 2A-B). In contrast, PLEKHG3 could not be detected in V5 immunoprecipitates from cells expressing V5-T-L3 or in the V5-CYTO and V5-LYSO controls (Figure 2C). These results indicated that PLEKHG3 is a transient interactor, or a proximal, not directly binding protein, of L3.

We next asked whether the interaction occurs at a specific subcellular localization. To address this question, we used HeLa cells, which are flatter than HEK cells and therefore more suitable for imaging. Similar to HEK cells, V5-T-L3 biotinylated the PLEKHG3 protein at nearly twice the efficiency of the control cytosolic decoy (Figure 2D-E).

PLEKHG3 and lysosomes colocalize at the PM independently of L3

In HeLa cells, endogenous PLEKHG3 localized to the PM where it colocalized with Phalloidin, as already reported in the literature (Figure 3A and S3A; and Nguyen et al., 2016), confirming the data from HEK293T cells shown in Figure S2C. GFP-PLEKHG3 stably expressed in HeLa cells showed a similar localization, but more clearly labeled filamentous actin, particularly cortical actin structures (Figure S3B-C). In addition, co-staining of endogenous PLEKHG3 and LAMP1, used as a late endosomes/lysosomes marker, revealed colocalization right below the PM (Figure 3-C). PLEKHG3 accumulation sites showed a strong enrichment of LAMP1 positive vesicles compared to PM regions low in PLEKHG3, and vice versa (Figure 3C). More

specifically, we found that PLEKHG3 colocalized more strongly with LAMP1-positive vesicles in elongated membrane structures (Figure 3D-E). Focal adhesion sites, which anchor the intracellular cortical actin network to the extracellular matrix and are remodeled with the help of late endosomes/lysosomes during protrusion formation and cell motility, can also be found in such elongated membrane protrusions (reviewed in Burridge and Burridge, 2017; Schiefermeier et al., 2014).

Immunofluorescence experiments showed the reported colocalization of endogenous PLEKHG3 (Figure S2C in HEK293T cells, Figure S3A in HeLa cells) and GFP-PLEKHG3 with cortical actin structures and the partial localization of LAMP1-positive vesicles to these structures in correspondence with vinculin-positive focal adhesions (Figure 3F). These findings provide further evidence for the association of PLEKHG3 with the actin cytoskeleton and lysosomal trafficking in our system.

In a next step, we investigated the possible influence of LAMTOR on this process using L3 KO cells. (Figure S3D). The knockout of L3 resulted in a strong reduction as well as in a complete dispersion of the LAMTOR4 signal from the lysosome (Figure S3E-F), as expected from earlier reports showing that loss of one LAMTOR subunit causes the disruption of the complex, its delocalization from the lysosome, and a destabilization of the other LAMTOR subunits (Nada et al., 2009; de Araújo et al., 2013). GFP and GFP-PLEKHG3 constructs were introduced in these cells and expressed at similar levels (Figure S3G). Both, GFP-PLEKHG3 and LAMTOR4 were found enriched in lysosomal structures at paxillin-positive FAs (Figure S3H-I). However, the association of GFP-PLEKHG3 with FA was not impaired in L3 KO cells, and the expression of GFP-PLEKHG3 did not impact the distribution of LAMTOR4-positive vesicles (Figure S3E-J).

Morphometric analysis of FA structures revealed a slight decrease of FA number in L3 KO cells, while the overall area and aspect ratio remained unaffected (Figure S3K). GFP-PLEKHG3 expression did not affect any of these parameters. Live imaging of cells expressing either GFP or GFP-PLEKHG3 clearly showed that L3 KO cells spread less compared to WT cells, while the expression of GFP-PLEKHG3 had no discernible effect on spreading (Movie S1-4 + Figure S3L).

FA as meeting hubs for PLEKHG3 and lysosomes

Based on the results above, PLEKHG3 is a proximal L3 protein rather than a transient physical interactor, and its biotinylation by L3 baits might reflect a previously undescribed interaction of PLEKHG3 with peripheral lysosomes at FA. Confirming the data in Figure S3H-I, GFP-PLEKHG3 and LAMP1-positive vesicles were found enriched in FA labeled by paxillin (Figure 4A-E). As expected, based on the enrichment of LAMTOR4 in FAs (Figure S3I) the LAMP1 signal was stronger in paxillin-labeled FA compared to control regions (Plot in Figure 4B).

To further investigate the colocalization of PLEKHG3 with late endosomes/lysosomes, we performed live cell imaging of GFP-PLEKHG3 cells incubated with LysoTracker to label acidic endo-lysosomal structures. Following a single cell over time, we could observe that a subset of lysosomes appears to travel to PLEKHG3 accumulation sites and specifically move into developing protrusions (Figure 4F + Movie S5).

These data are consistent with the hypothesis that lysosomes moving in an anterograde manner reach FA sites (Schiefermeier et al., 2014) where they encounter PLEKHG3, and successively travel in PLEKHG3-induced protrusions.

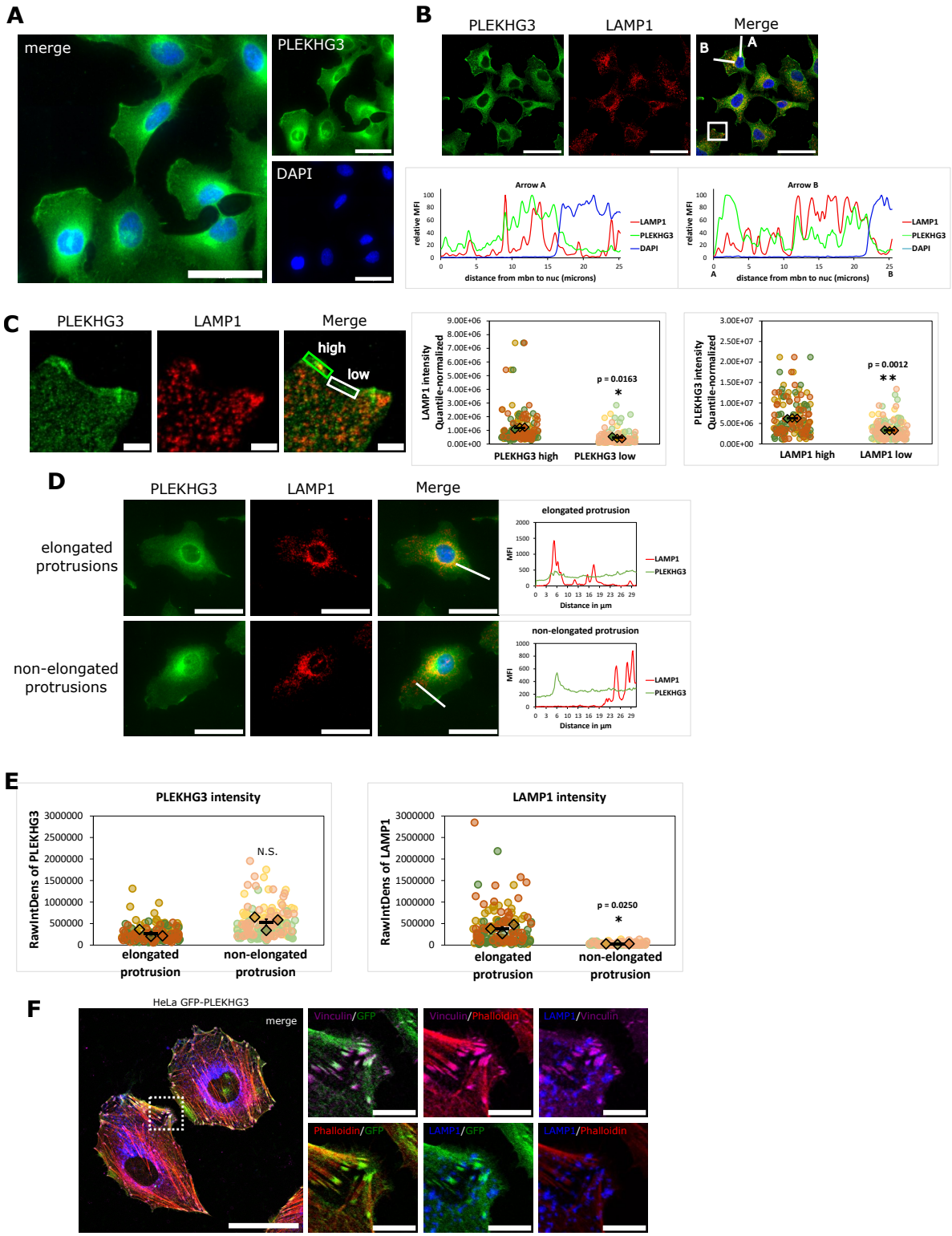

Figure 3: PLEKHG3 and lysosomes colocalize at protrusions in the cell periphery. A) Immunofluorescence images of HeLa cells stained for endogenous PLEKHG3 (green) and DAPI (blue). Scale bar = 50 µm. **B)**

Immunofluorescence images of HeLa cells stained with PLEKHG3 (red) and LAMP1 (grayscale) antibodies show an enrichment of lysosomes at PLEKHG3-high regions of the PM. White lines are drawn from the extracellular space to the nucleus, either over a PLEKHG3-high region (line A) or over a PLEKHG3-low region (line B) of the PM. The intensity of the PLEKHG3/LAMP1 staining is shown in profile plots below the images; scale bar = 50 µm **C)** Higher magnification of the PM region boxed in white in B. This a representative image showing PLEKHG3-high regions outlined in green, PLEKHG3 low regions in white; scale bar = 5 µm. Images were acquired on Olympus slide scanner. **D)** PLEKHG3 and LAMP1 content in elongated (top panels) or non-elongated protrusions (bottom panels). Endogenous PLEKHG3 is shown in red, LAMP1 in grayscale. Scale bar = 30 µm. The profile plots (right) show PLEKHG3 and LAMP1 intensity along the white lines drawn on the merged images. **E)** Quantification of PLEKHG3 and LAMP1 intensity in elongated vs. non-elongated protrusions. Images in A-D were acquired on Olympus slide scanner. **F)** Confocal immunofluorescence image of HeLa cell stably expressing GFP-PLEKHG3 and immunostained with LAMP1 (lysosomes), Vinculin (FAs) and stained with Phalloidin (F-actin). Scale bar = 50 µm. Insets show indicated channels to better visualize colocalization events. Scale bar = 10 µm. **A-D** show epifluorescence images. In the superplots in **C and E,** dots represent individual data points of each of the three-color coded replicates; diamonds represent the mean of each replicate; black bars represent the mean ± the SEM of three biological replicates; * = p values according to student's t-test.

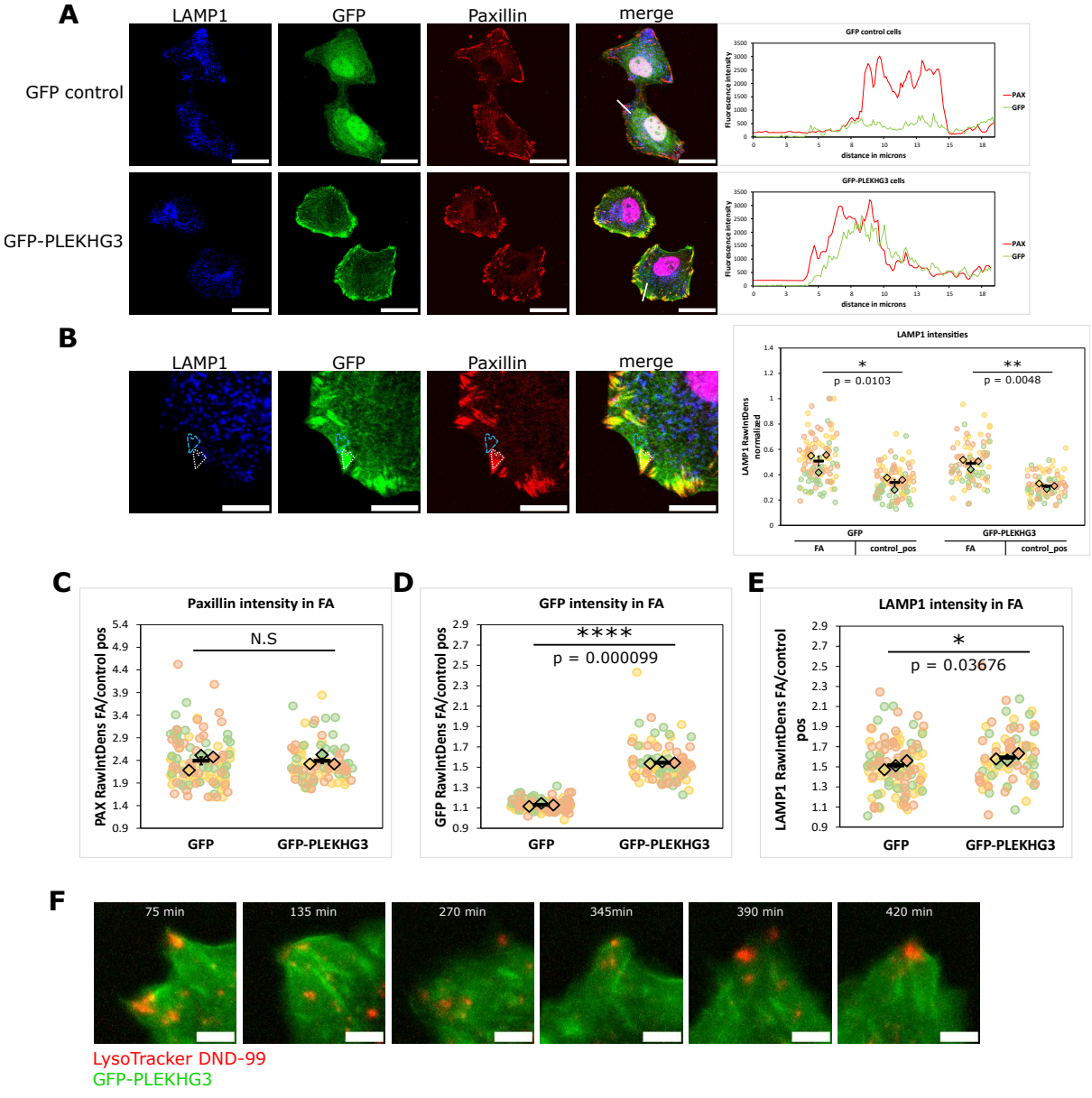

Figure 4: PLEKHG3 accumulates and colocalizes with lysosomes at FA sites. A) Confocal images of HeLa cells stably expressing GFP or GFP-PLEKHG3 (green). Cells were stained with Paxillin antibodies (red) to label FAs and with LAMP1 antibodies (grayscale) to label late endosomes/lysosomes. White lines correspond to profile plots on the right. Scale bar = 30 µm. **B)** Confocal images for schematic representation of colocalization analysis. HeLa cells stably expressing GFP-PLEKHG3 were stained with Paxillin and LAMP1 antibodies as described above. PLEKHG3 and LAMP1 intensity was measured in FAs, identified using the Pax channel (dotted white line), and in adjacent, Pax-negative positions of similar shape and area (control positions, broken blue line; see materials and methods section for details) Scale bar = 10 µm. **C-E)** GFP/PAX/LAMP1 colocalization. Average intensity of the respective fluorophores in an average of 50 FA per cell. In the superplots, dots represent individual data points of each of three color coded biological replicates of experiments similar to the one shown as immunofluorescent image; diamonds represent the mean of each replicate; black bars represent the mean ± the SEM of the three biological replicates; * = p values according to student's t-test. **F)** Epifluorescence stills from Movie S5. LysoTracker DND-99 in red and GFP-PLEKHG3 in green show lysosomal movement into cell protrusions. Images were acquired every 15 minutes on a Zeiss Celldiscoverer 7.

Lysosomal trafficking impacts PLEKHG3 localization

The colocalization of PLEKHG3 with peripheral lysosomes raised the question of whether lysosomal trafficking affected the subcellular localization of PLEKHG3.

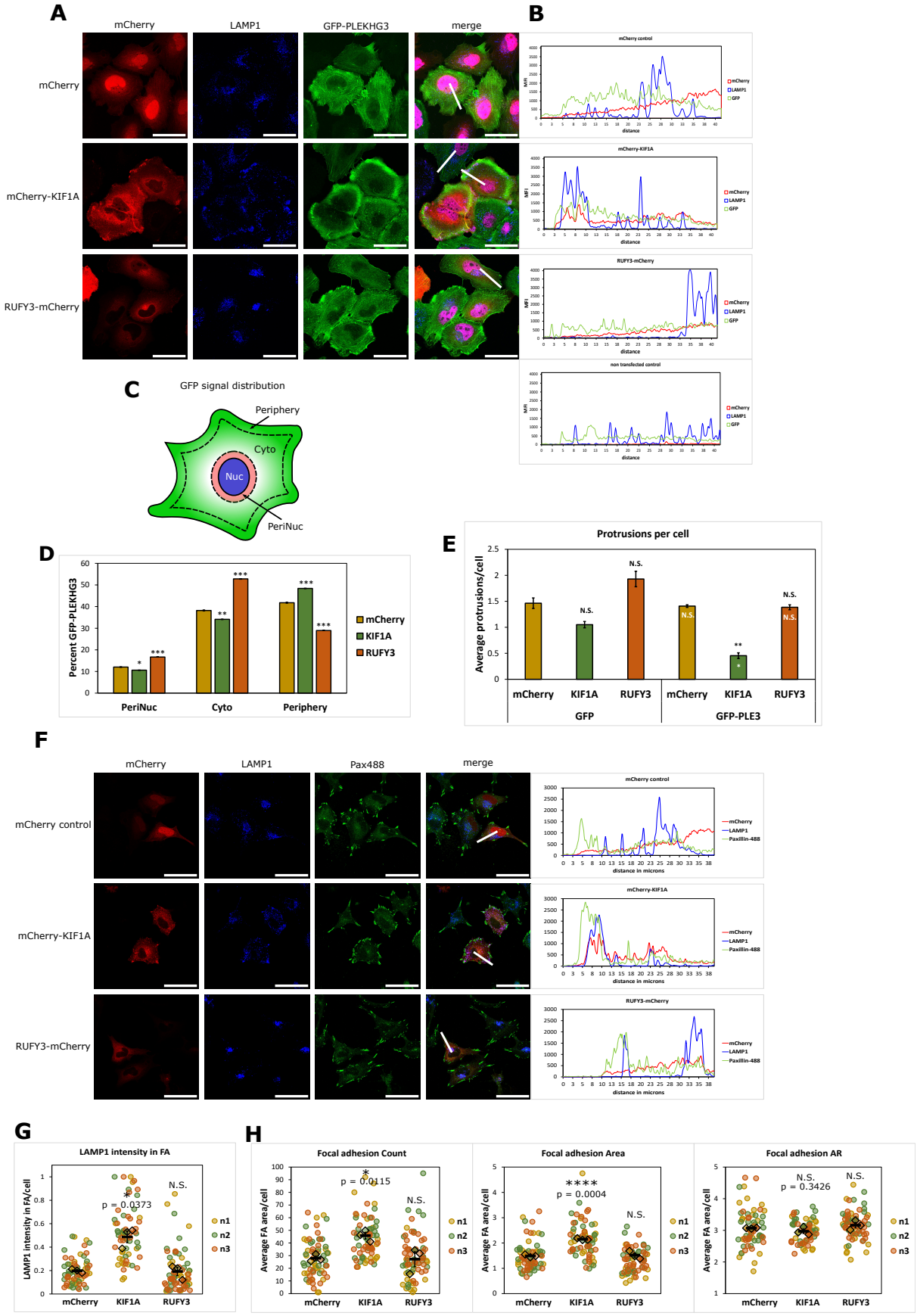

Figure 5: Effect of lysosomal positioning on PLEKHG3 and FAs. A-B) Confocal immunofluorescence images of HeLa cells stably expressing GFP-PLEKHG3, transfected with mCherry constructs (red) and stained with a LAMP1

antibody (grayscale) as well as with DAPI (blue) after fixation. Scale bar = 50 µm. The line plots on the right (B) indicate the distribution of GFP-PLEKHG3, LAMP1 and mCherry along the white lines drawn from the PM to nucleus. **C)** Schematic representation the distribution analysis. Cells were segmented in Periphery, cytosolic (Cyto) and perinuclear (PeriNuc) regions. GFP intensity was measured in all three segments and the percentage of GFP in each segment was calculated using the intensity of all three segments as 100%. For details see materials and methods. **D)** Quantification of GFP-PLEKHG3 distribution in three independent experiments similar to the one shown in A based on scheme in C. GFP-PLEKHG3 intensity became significantly higher towards the PM. Error bars = SEM. * = p values according to student's t-test. **E)** Average protrusion number per cell in three independent experiments similar to the one shown in A. Black asterisks = p values according to student's t-test, comparing the effect of KIF1A or RUFy3 expression with the effect of mCherry. White asterisks in the bars indicate the p values according to student's t-test comparing GFP-PLEKHG3 and GFP expressing cells. **F)** Confocal immunofluorescence images of HeLa cells expressing the indicated mCherry constructs and immunostained for LAMP1 (grayscale) and Paxillin (green). Scale bar = 50 µm. The line plots on the right indicate the distribution of mCherry, LAMP1 and Pax the white lines drawn from the PM to nucleus. **G)** Lysosomal content in Pax-positive FAs. KIF1A overexpression significantly increases LAMP1 accumulation in FA structures. Superplots show average LAMP1 intensity in FAs per cell. **H)** Morphometric analysis of focal adhesions. KIF1A overexpression increased FA numbers and area. **G-H**, dots represent individual data points of each of three color coded biological replicates of experiments similar to the one shown in F; diamonds represent the mean of each replicate; black bars represent the mean ± the SEM of the three biological replicates; * = p values according to student's t-test.

To answer this question, we altered lysosomal localization using RUFY3-mCherry to promote lysosomal inward transport (Keren-Kaplan et al., 2022; Kumar et al., 2022), and mCherry-KIF1A to drive lysosomal centrifugal dispersion (Guardia et al., 2016). Overexpression of mCherry-KIF1A in GFP-PLEKHG3 expressing stable cell lines induced a concentration of GFP-PLEKHG3 in the cell periphery (Figure 5A-B, profile plots in B, Figure S4A-C). To quantify this effect, we segmented the cytoplasm into 3 areas (perinuclear = PeriNuc, cytoplasm = Cyto, Periphery) and calculated the percentage of PLEKHG3 in each segment by setting the intensity measured in all three segments to 100 % (Figure 5C). While in RUFY3-mCherry the maximum GFP-PLEKHG3 intensity was found in the cytoplasm, in mCherry-KIF1A expressing cells there was a clearly detectable increase towards the periphery (Figure 5D). As a control, the expression of mCherry, mCherry-KIF1A, or RUFY3-mCherry had no effect on the localization of GFP (Figure S4D-E). The effect of the peripheral accumulation of lysosomes on PLEKHG3 distribution could be confirmed by visualizing endogenous PLEKHG3 in cells transiently expressing KIF1B (Figure S4F-H). LAMP1 accumulation sites showed a slight increase in

endogenous PLEKHG3 compared to control regions, and vice versa (Figure S4I-K). Concentration of GFP-PLEKHG3 at the PM by mCherry-KIF1A overexpression, however, did not increase the number of protrusions (Figure 5E), in contrast to the reported positive effect of this protein on actin remodeling (Nguyen et al., 2016). Quantification of protrusions clearly indicated a drop upon overexpression of mCherry-KIF1A compared to mCherry control or RUFY3-mCherry overexpression. This effect, consistently present as a trend in GFP control cells, became strongly significant in GFP-PLEKHG3 expressing cells. Concentration of lysosomes around the nucleus by overexpression of mCherry-RUFY3 had no significant effect on protrusion number compared to control conditions (Figure 5E).

In terms of morphology, the cells expressing mCherry-KIF1A exhibit a higher circularity and a lower aspect ratio compared to mCherry control or RUFY3-mCherry expressing cells, although the cell area remained unaffected (Figure S4L-N). In addition, as previously described (Guardia et al., 2016) KIF1A redirected lysosomes to FA sites (Figure 5F-G), which might suggest increased FA remodeling (Schiefermeier et al., 2014; Pu et al., 2017). Instead, overexpression of mCherry-KIF1A resulted in higher numbers and larger size of FAs compared to both the mCherry control and RUFY3-mCherry (Figure 5F + H). Together with their rounder morphology, this might suggest a reduced propensity of KIF1A overexpressing cells to form protrusions and/or move.

Forced peripheral dispersion of lysosomes impacts motility and membrane protrusive activity

We next performed live cell imaging experiments to investigate the effects of the manipulation of lysosomal positioning on protrusion formation, cell motility, and on the

subcellular localization of GFP-PLEKHG3 (Supp Movies S6-11, Figure 6A). Cells expressing mCherry-KIF1A were not only rounder than mCherry control and RUFY3-mCherry expressing cells, but also barely moved, in contrast to the other cells, particularly the RUFY3-mCherry expressing cells, which were very motile. Morphometric analysis performed over a time span of 128 min revealed that KIF1A and RUFY3 slightly increased cell size in the GFP cell line; the most evident increase in size, however, was caused by GFP-PLEKHG3 itself, particularly when co-expressed with RUFY3 (Figure 6B). GFP-PLEKHG3 also promoted circularity, even more so upon co-expression of mCherry-KIF1A, confirming the experiments in fixed cells (Figure 5A + Figure S4M). Accordingly, analysis of the aspect ratio of the cells averaged over time showed that mCherry-KIF1A caused a decrease, while RUFY3 caused a slight increase in this parameter, which was not impacted by GFP-PLEKHG3 expression (Figure 6D).

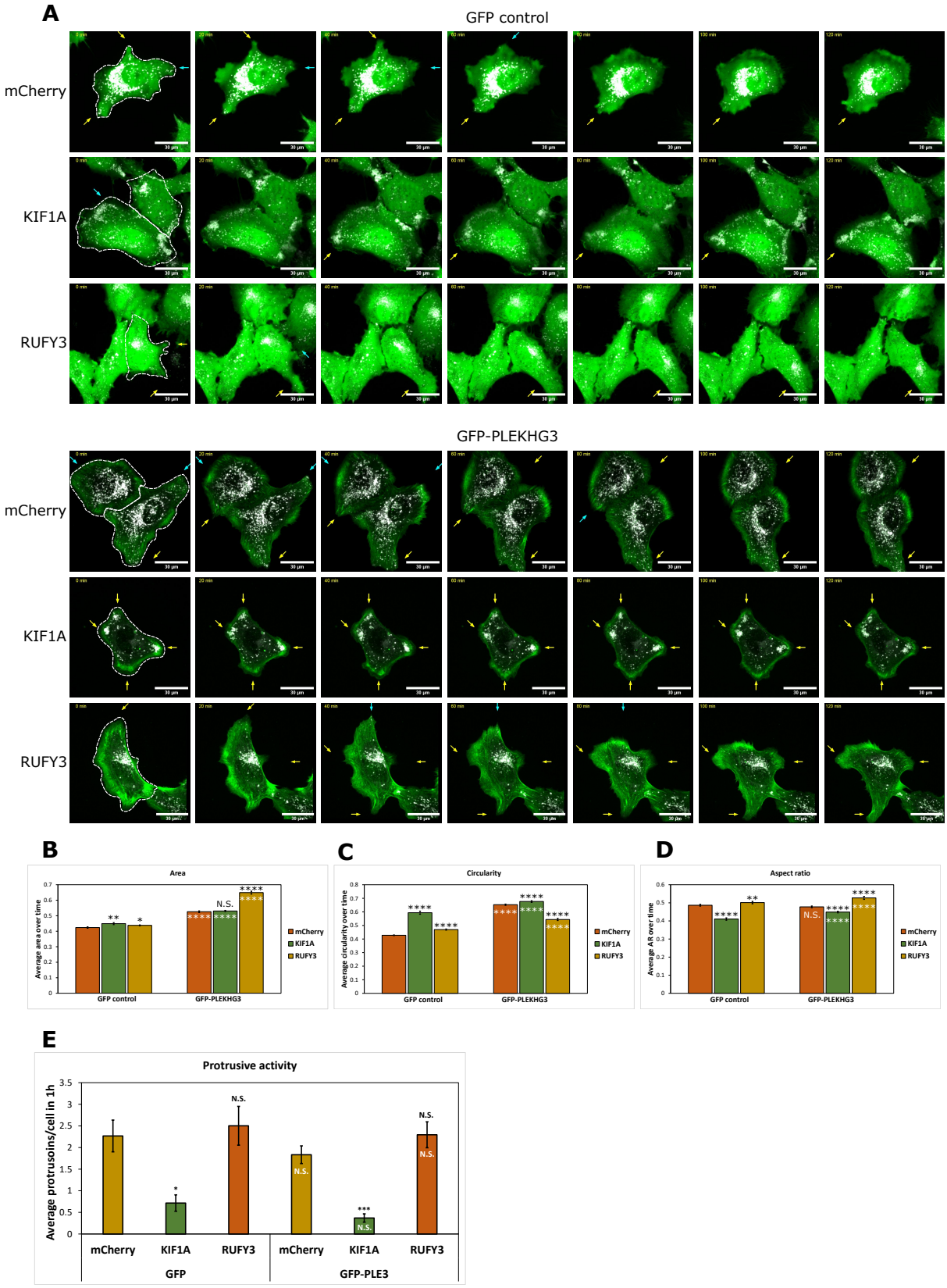

Figure 6: Peripheral clustering of lysosomes inhibits protrusion formation. A) Stills from live cell imaging (Movies S6-11). Cells stably expressing GFP or GFP-PLEKHG3 were transfected with the indicated mCherry constructs. Successfully transfected cells are contoured by a white broken line in the first still image. Yellow arrows = forming protrusions; blue arrows = retracting protrusions. Stills were generated over a period of 2 hrs. Scale bar = 30 µm. **B-D)** Morphometric analysis of cells over time. Cell shape analysis was performed with Fijis shape descriptors (see materials and methods) per cell every four minutes. Bar plots represent the average over

all time points to represent changes in shape over time. **E)** Quantification of protrusions formed and retracted over time in cells from A. Values indicate average number of protrusions formed in a timespan of one hour from a total of ≥ 19 cells per condition. Error bars = SEM. In **B-E,** black asterisks denote p values according to student's t-test, comparing the effect of KIF1A or RUFY3 expression with the effect of mCherry. White asterisks in the bars indicate the p values according to student's t-test comparing GFP-PLEKHG3 and GFP expressing cells.

Analysis of the number of forming protrusions and retracting membranes, averaged over a one-hour timespan, revealed a significant decrease in protrusion formation upon overexpression of mCherry-KIF1A. This effect was further exacerbated in cells expressing GFP-PLEKHG3 (Figure 6E), thereby confirming the results presented in Figure 5E.

Discussion

In this study, we identify PLEKHG3 as a vicinal protein of L3 by proximity-dependent labeling and show that GFP-PLEKHG3 accumulates at FAs, where it colocalizes with peripheral lysosomes. We demonstrate that peripheral clustering of lysosomes concentrates PLEKHG3 at the PM, but at the same time inhibits protrusion formation, decreasing overall cell motility.

The proximity labeling screen correctly identified most of the proteins known to associate with the LAMTOR complex (Figure 1D). However, both lysosomal baits, L3 and TMEM192, failed to biotinylate LAMP1, a very abundant lysosomal transmembrane protein. This is in line with a BioID screen performed by Go et al. in HEK293 cells (Go et al., 2021), who showed that LAMP1 was not biotinylated by a LAMTOR1 bait and vice versa. This supports the view that the proteins at the lysosome's membrane are spatially compartmentalized into distinct subdomains.

Similarly, TMEM192 missed several of the proteins labeled by L3, including the prominent biotinylated PLEKHG3. This could be explained by the fact that TMEM192 features only a small cytosolic tail and thus doesn't reach as far into the cytoplasm as L3, which is more distal from the membrane (Nguyen et al., 2017; de Araujo et al., 2017). Be that as it may, labeling of PLEKHG3 by L3 did not reflect a stable interaction (Figure 2A, C-D), and L3 KO in turn did not have an influence on PLEKHG3 distribution (Figure S3E-H, Movie S1-4). Therefore, PLEKHG3 is a vicinal protein of L3.

PLEKHG3 colocalizes with lysosomes at FA sites

PLEKHG3 has previously been shown to localize to both the leading and the trailing edge of migrating cells, where remodeling of the actin cytoskeleton takes place, and to associate with freshly polymerized actin via its actin-binding domain (Nguyen et al., 2016). Our experiments

confirm this localization of GFP-PLEKHG3 to cortical actin, but in addition show that PLEKHG3 is specifically enriched at FA sites in HeLa cells (Figure 3A + Fig 4B-D). During protrusion formation, new FAs are formed by extracellular matrix/integrin interaction. These nascent adhesions connect to actin fibers and further mature to FAs (reviewed in Gardel et al., 2010). The connection with growing actin fibers may be the basis of the accumulation of PLEKHG3 around FAs.

In line with published evidence (Guardia et al., 2016), we also find an enrichment of peripheral lysosomes at FA sites (Figure 4B-E), where they fulfil a number of functions, including the control of FA dynamics by IQGAP release from FA complexes (Schiefermeier et al., 2014) or by dissolution of extracellular matrix/Integrin complexes (Dykes et al., 2016; Mohamed and Sloane, 2006).

The observation that PLEKHG3 and LAMP1-positive vesicles were in close proximity to one another at FA and protrusion sites (Figure 4B-E, Figure 3C-F) led to the hypothesis that PLEKHG3 biotinylation by L3 was the result of dynamic encounters at sites of protrusion formation and prompted us to ask whether association with the lysosomes or lysosomal trafficking had any impact on PLEKHG3 distribution. Indeed, the effect was profound (Figure 5A-D). Driving lysosome outward transport by overexpression of KIF1A promoted the redistribution of both GFP-PLEKHG3 and of endogenous PLEKHG3 to the periphery of the cell. Whether the lysosomes are directly responsible for the transport of PLEKHG3 to the membrane is difficult to determine, since both endogenous and exogenous PLEKHG3 accumulated at protrusions which frequently harbored lysosomes but could also be found at sites that contained very few to no lysosomes (Figure 3G-H). Promoting the translocation of lysosomes to the periphery did not increase protrusive activity. Rather, we observed the opposite effects: cells became rounder, less protrusions formed, and the overall cell motility

decreased. Clustering of lysosomes around the nucleus by RUFY3 had the opposite effect both on PLEKHG3 distribution and cell morphology/motility (Figure 5E + Figure S4L-N).

The negative effect of KIF1A and PLEKHG3 overexpression on protrusion activity and cell motility was unexpected in two respects: firstly, PLEKHG3 overexpression has been shown to promote protrusion activity (Nguyen et al., 2016); and secondly, centrifugal trafficking of lysosomes towards the periphery has been shown to contribute to protrusion activity, spreading and motility (Pu et al., 2017; Filipek et al., 2017; Marwaha et al., 2022 *Preprint*). Lysosomes can contribute to protrusion formation by delivering membranes and actin polymerization-promoting factors to the newly formed structures (reviewed in Garcin and Straube, 2019; Steffan et al., 2010; Johnsson and Karlsson, 2010; Condeelis and Singer, 2005). Integrins, for instance, have been shown to travel via the late endosome/lysosome route to the periphery where they aid to establish new FAs and thereby promote protrusion formation (Lawson and Maxfield, 1995; Dozynkiewicz et al., 2012). In line with the latter, we identified an increased number and size of FAs in cells overexpressing KIF1A (Figure 5E + G), which might contribute to a more static cellular behavior. It is likely that upsetting the balance between anterograde and retrograde transport of lysosomes within the cell prevents the removal and degradation of membrane components involved in FA dynamics (e.g. integrins) and/or in the actin remodeling necessary for protrusion formation and motility. As an example, it has recently been reported that lysosomes remove the GDP-bound, inactive form of the PLEKHG3 downstream effector Rac1 from the vicinity of the PM in order to increase the concentration of GTP-bound, active Rac1 at the leading edge, thus promoting cell migration (Marwaha et al., 2022 *Preprint*).

In this situation of impasse, PLEKHG3 might be recruited to the PM, but this alone might not be sufficient to promote protrusion activity and cell motility.

Taken together, our results identify PLEKHG3 as a new L3 vicinal protein that encounters lysosomes at FAs, revealing a previously undiscovered interplay between lysosomal trafficking and PLEKHG3 distribution/protrusion-promoting function. The data highlight the unique potential of PDL-based approaches to discover interactions between molecules, or as shown here between molecules and intracellular structures, that are physiologically relevant but limited in space and time.

Materials Methods

Cell culture

Human embryonic kidney (HEK) 293T, Flp-In™ T-REx™ 293 (Invitrogen™) and Human HeLa cervical carcinoma (HeLa) cells were cultured in DMEM (D5796; Sigma-Aldrich) supplemented with 10% FBS, and 100 U/ml penicillin–streptomycin at 37°C, 5% CO2. Stable GFP and GFP-PLEKHG3 HeLa cells were cultured under similar conditions with 100 µg/ml hygromycin B (H3274; Sigma-Aldrich).

Transfection

Transfections were performed with 1 µg DNA in 6-well plates and 400 µg DNA in 24-well plates. Cells were starved in serum-free medium for 30 min prior to transfection. DNA and PEI transfection reagent were incubated and mixed in plain DMEM (D5796; Sigma-Aldrich). Starvation medium was exchanged with 9 parts full medium and 1 part transfection mix. Cells were incubated for about 24 hours at culture conditions.

siRNA-based knockdown

Oligo duplex siRNA against human PLEKHG3 (SR308671) were purchased from OriGene. Final siRNA concentrations of 20, 40 or 60 nM were used for silencing (indicated in figures) and incubated for 36-48 hours. Transfections were performed using Lipofectamine™ RNAiMAX transfection reagent (Invitrogen; 13778-150) according to manufacturer's instructions.

Generation of DNA constructs and stable cell lines

Genes of interest for transient transfection were cloned into a pCDNA3.1 vector by Gibson assembly. In brief, pCDNA3.1 vector was linearized by restriction digested with BamHI and

EcoRI. mCherry insert was amplified by PCR from pcDNA5-MTS-TagBFP-P2AT2A-EGFP-NLS-P2AT2A-mCherry-PTS1 (87829; Addgene) using the primers 5'-caagcttggtaccgagctcggatccATGGTGAGCAAGGGCGAG-3' (forward) and 5'-agtgtgatggatatctgcagaattcttaCTTGTACAGCTCGTCCATGC-3' (reverse); mCherry-KIF1A insert was amplified from pCW57.1-mCherry-KIF1A (inhouse, built from eGFP-KIF1A (172206; Addgene)) using the primers 5'-caagcttggtaccgagctcggatccgccaccATGGTGAGCAAGGGCGAG-3' (forward) and 5'-agtgtgatggatatctgcagaattcTCAGACCCGCATCTGCGC-3' (reverse); RUFY3-mCherry insert was PCR amplified from RUFY3 cDNA with primers 5'-caagcttggtaccgagctcggatccGCCACCATGTCTGCTCTG-3' (forward) and 5'-tgctcaccatTCCTCCTGATGGGCTGGTAG-3' (reverse) and mCherry from pcDNA5-MTS-TagBFP-P2AT2A-EGFP-NLS-P2AT2A-mCherry-PTS1 (87829; Addgene) using the primers 5'-atcaggaggaATGGTGAGCAAGGGCGAG-3' (forward) and 5'-agtgtgatggatatctgcagaattcTTACTTGTACAGCTCGTCCATG-3' (reverse). All inserts were fused into pCDNA3.1 backbone by Gibson assembly according to the manufacturer's instructions. pEGFPC1-KIF1B was constructed by Gibson assembly of PCR amplified human KIF1B derived from cDNA using the primers 5'-gatctcgagctcaagcttcgaattctATGTCGGGAGCCTCAGTG-3' (forward) and 5'-tcagttatctagatccggtggatccTTAGTATTTCGACTGGCTCGG-3' (reverse) with BamHI and EcoRI digested pEGFPC1 backbone. GFP and GFP-PLEKHG3 plasmids were constructed by Gibson assembly of BamHI and EcoRI restriction digested pCSII-hygro backbone with GFP using the primers 5'-acacgctaccggtctcgacgaattcGCCACCATGGTGAGCAAG-3' (forward) and 5'-ctagcttaagttagttaacggatccTCACTTGTACAGCTCGTCC-3' (reverse) or GFP-PLEKHG3 from pEGFP-GFP-PLEKHG (inhouse) using the primers 5'-acacgctaccggtctcgacgaattcGCCACCATGGTGAGCAAG-3' (forward) and 5'-

ctagcttaagttagttaacggatccTCAACCGACAGAGTTCAAGG-3' (reverse). Stable HeLa cells expressing GFP or GFP-PLEKHG3 were generated by lentiviral transduction and maintained in hygromycin B selection (100 µg/mL). L3 KO cell lines were generated using the CRISPR/Cas9 protocol (Ran et al., 2013). In brief, three L3 guides were designed with the benchling CRISPR online tool two of which located in exon 4 (ATCTCTATCTGACACAACAA; TATCTGACACAACAATGGCA) and one in exon 5 (GCAAAAGTGGATAAGAAACC). Single guide RNAs were cloned into pSpCas9(BB)-2A-GFP (PX458) (48138; Addgene) and transfected into HeLa cells. 24 hours post transfection cells were sorted via FACS (FACS Melody) for FITC-positive cells. Bulk sorts were expanded and analysed via Western blot for successful L3 deletion. A second round of transfection was necessary to achieve a 95-99% reduction in L3 expression.

Immunofluorescence

Immunofluorescence was performed as follows: Cells were fixed in 4% formaldehyde in PBS for 10 min, washed three times with 1x PBS and permeabilized with 0.02% Saponin + 3% BSA (w/v) in PBS for 20 min at room temperature. The following primary antibodies diluted in permeabilization solution were used for incubation overnight at 4 °C: rabbit anti-V5 (1:500; #13202), rabbit anti-LAMP1 (1:500; #9091; used in Figures 3F, 4A-B, S3G), rabbit anti-LAMTOR4 (1:500; #13140) were purchased from Cell Signaling Technology; rabbit anti-V5 tag (1:500; V8137) and mouse anti-Vinculin (1:400; V9131) from Sigma-Aldrich; additional antibodies were rabbit anti-PLEKHG3 (1:200; PA5-66764; Invitrogen), mouse anti-paxillin (1:200; 610055; BD Biosciences, discontinued project; used in Figures 4A-B, S3G), rabbit anti-Paxillin (1:1000; ab246718; Abcam; used in Figure 5F) and mouse anti-LAMP1 (1:500; sc-20011; Santa Cruz; used in Figures 1B-D, 5A + F, S1F, S2C, S3A + D, S4D + F + I) and. Cells were washed three times with 1x PBS and incubated with the appropriate secondary antibodies

conjugated with Alexa Fluor 488, 594, 647, 568 (1:1,000; Thermo-Fisher Scientific) and Alexa Fluor 405 (1:250; Thermo-Fisher Scientific) for 1 h at room temperature. After incubation with DAPI for 10 min (in some cases without DAPI) coverslips were mounted on glass slides with Prolong Gold antifade reagent (P36934; Thermo-Fisher Scientific). Confocal images were captured on an LSM 700 microscope (Zeiss) using a 40x Plan-Apo/1.3 NA oil objective at room temperature with a PMT detector. The acquisition software was Zeiss ZEN 2012 SP5. For medium throughput imaging (indicated in figure legends) slides were imaged on a Slide Scanner VS120 (Olympus) with a 40x dry objective and a CCD camera via the software OlyVIA. High content screening was performed at TIGEM (Naples, Italy) on an Operetta (PerkinElmer) equipped with a Spinning Disk confocal setup using a 20x/0.4 NA air objective and a sCMOS camera at room temperature. All images were analysed in ImageJ by determining regions of interest (ROIs) in the respective channels. Images are presented with adjusted brightness and contrast. The same adjustments were made in ImageJ for every experiment.

Live cell imaging

Prior to imaging cells were incubated with 60 nM LysoTracker Red DND-99 (L7528, Invitrogen) or 50 nM LysoTracker Deep Red (L12492, Invitrogen) in imaging DMEM (31053-028; Gibco) without phenol red supplemented with 10% FCS and 2% L-glutamine for 30 min at 37 °C in precoated 4- or 8-well ibidi glass bottom chambers. Cells were subsequently imaged under a Live Spinning Disk microscope (Visitron) using a Plan Apo Lambda 60x/1.42 NA oil objective at 37 °C, 5% CO_2. Images were acquired depending on the experiments with 488, 561 and 640 lasers for GFP, mCherry and LysoTracker Deep Red, respectively on an EM-CCD camera. Images were taken every 4 minutes on multiple positions for a time course of 2-3 hours. Software used was VisiView. Where indicated, cells were imaged on a Celldiscoverer 7 (Zeiss)

using a Plan-Apochromat 50x/1.2 NA water-immersion objective at 37 °C, 5% CO_2 taking images every 15 min. Images were acquired with a Hamamatsu ORCA Flash4.0 V2 sCMOS camera using the software Zeiss ZEN 3.1. All movies were processed in ImageJ. For presentation purposes z-projections of videos with constant contrast and brightness adjustments in every experiment are shown.

Immunoblotting

Immunoblotting was performed as follows: Cells were washed three times in ice cold PBS (D8537; Sigma-Aldrich) and lysed in RIPA buffer (50 mM Tris-HCl, pH 7.4, 150 mM NaCl, 1% Triton X-100, 0.5% sodium deoxycholate, and 0.1% SDS) supplemented with cOmplete™, Mini, EDTA-free protease-inhibitor cocktail (40694200; Roche) on ice. Protein concentrations of lysates were measured using a Pierce™ BCA protein assay kit (23225; Pierce), and equal amounts of protein (30 µg) were subjected to SDS-PAGE and immunoblotted. The following primary antibodies were incubated on membranes overnight at 4°C: rabbit anti-LAMTOR1 (1:1000; #8975), rabbit anti-L3 (1:1000; #8168), rabbit anti-LAMTOR4 (1:1000; #13140), rabbit anti-LAMTOR5 (1:1000; #14633), rabbit anti-RAPTOR (1:1000; #2280), rabbit anti-AMPK (1:1000; #2532), rabbit anti-RagC (1:1000; #9480), rabbit anti-GFP (1:1000; #2956), rabbit anti-V5 (1:4000; #13202) all from Cell Signaling Technology; rabbit anti-PLEKHG3 (1:1000; PA5-66764), Streptavidin-HRP (1:2500; 434323) were from Invitrogen; rabbit anti-PLEKHG3 (1:1000; HPA063455), mouse anti-α-Tubulin (1:10,000; T5168) were from Sigma-Aldrich and other antibodies were rabbit anti-mCherry (1:2000; 26765-1-AP; Proteintech),rabbit anti-RUFY3 (1:1000; LS-C681236; LSBio), rabbit anti-PLEKHG3 (1:1000; AP11167b; Abcepta), rabbit anti-GAPDH (1:10,000; ABS16) from Merck and rabbit anti-TMEM192 (1:100; ab236858; Abcam). Secondary antibodies (Jackson ImmunoResearch) were

all conjugated to horseradish peroxidase and incubated at a dilution of 1:5000 for 1h at room temperature. SuperSignal™ West Pico PLUS ECL reagent (34580; Thermo-Fisher Scientific) was used to visualize chemiluminescence on a ChemiDoc imaging system (Bio-Rad Laboratories). Quantification of Western blots was performed where indicated using ImageJ (version 1.41; National Institutes of Health).

Pulldowns and immunoprecipitations

Streptavidin-pulldowns were performed as follows: All cells were incubated with 500 µM Biotin (Sigma-Aldrich; B4501) for 10 min in medium containing 10% FCS. Subsequently, cells were washed thrice with ice cold 1x phosphate buffered saline (PBS) (TMS-012; Sigma-Aldrich). HeLa cells were rinsed in the dish while kept on ice and HEK293T or T-REx cells were carefully scraped from the plate and spin-washed in 15 ml falcon tubes in a table-top centrifuge at 300 rcf, 4 °C for 5 min. After the last washing step supernatant was aspirated and cells were lysed in RIPA lysis Buffer (50 mM Tris-HCl, pH 7.4, 150 mM NaCl, 1% Triton X-100, 0.5% sodium deoxycholate, and 0.1% SDS) supplemented with cOmplete™, Mini, EDTA-free protease-inhibitor cocktail (40694200; Roche). After protein concentration determination by BCA protein assay kit (23227; Thermo-Fisher Scientific) 300 µg protein in 600 µl total volume was incubated with 30 µl prewashed Streptavidin magnetic beads (88817; Pierce) at 4 °C overnight on a rotating wheel. For input samples 5-15 µg were used. After incubation 5-15 µg of supernatant were drawn from samples. Beads were washed three times with RIPA lysis buffer and eventually proteins were eluted from beads in 2x sample buffer by vigorously vortexing at room temperature. Samples were then boiled for 7 min at 95 °C and subsequently subjected to Western blot analysis.

Immunoprecipitations were performed in a similar manner: In brief, cells were also washed three times in ice cold PBS (rinse for Hela cells, spin-wash for T-REx cells) and lysed in ice cold IP lysis buffer (20 mM TRIS-HCl, 137 mM NaCl, 1 mM $CaCl_2$, 1 mM $MgCl_2$, 1% Triton X-100, 2 mM sodium-fluoride, 2 mM Phenylmethylsulfonylfluoride, 1 mM sodium-orthovanadate) supplemented with cOmplete™, Mini, EDTA-free protease-inhibitor cocktail (40694200; Roche). After protein concentration measurement the 300 µg of protein were incubated with 30 µl of anti-V5 tag magnetic beads (MBL International Corporation; M167-11) overnight at 4 °C on a rotating wheel. Further sample processing was equal to the above explained.

Treatments for TurboID screen

Amino acid starvation (EBSS) was performed by incubation in EBSS medium (14155048; Gibco) supplemented with 200 mg/L $CaCl_2$ + 200 mg/L $MgCl_2$ for 30 min. Restimulation (HF) was achieved by exchanging starvation medium with full medium containing 10% FCS for 10 min. FM condition was performed by incubation with medium containing 10% FCS for 50 min prior to lysis.

TurboID-based proximity-dependent labeling

pCDNA5_GOI FRT/TO (FLP recombination target/TetO) plasmids were constructed using the NEBuilder assembly tool (version 2.7.1; New England Biolabs) and generated by Gibson assembly according to the manufacturer's instructions (New England Biolabs; E2611S). In brief, pCDNA5 FRT/TO vector was cut open by restriction digestion with XhoI and BamHI. V5-TurboID-L3 insert was generated by PCR amplification from pCW57.1-V5-TurboID-L3 (inhouse) plasmid using the primers 5'-taagcttggtaccgagctcggatccAGCCACCATGGGCAAGCC-3' (forward) and 5'-

tttaaacgggccctctagactcgagTTAAGACACTTCCACAACTTTTATCAGTTCTTCAAATAAC -3' (reverse). V5-TurboID-TMEM192 insert was generated by separately PCR amplifying V5-TurboID insert from pCW57.1-V5-TurboID-L3 plasmid (inhouse) using the primers 5'-taagcttggtaccgagctcgGCCACCATGGGCAAGCCC-3' (forward) and 5'-cccccgccgcCTGCAGCTTTTCGGCAGACC-3' (reverse) and the TMEM192 insert from pLJC5-TMEM192-2xFLAG (102929; Addgene) using the primers 5'-aaagctgcagGCGGCGGGGGGCAGGATG -3' (forward) and 5'-tttaaacgggccctctagacTTACGTTCTACTTGGCTGACAGCCCAGGTC-3' (reverse). The V5-TurboID-NES insert was generated by PCR amplification from V5-TurboID-NES_pCDNA3 (107169; Addgene) using the primers 5'-taagcttggtaccgagctcggatccAGCCACCATGGGCAAGCC-3' (forward) and 5'-tttaaacgggccctctagactcgagTTAGTCCAGGGTCAGGCGC-3' (reverse). Inserts were mixed with the linearized pCDNA5 FRT/TO vector and fused by Gibson assembly. Stable T-REx cells were generated by using the Flp-In™ T-REx™ Core Kit (K650001; Invitrogen) according to the manufacturer's instructions. FlpIn T-REx host cells were transfected with pcDNA5-V5-TurboID-L3 FRT/TO, pcDNA5-V5-TurboID-TMEM192 FRT/TO or pcDNA5-V5-TurboID-NES FRT/TO and pOG44 at a ratio of 400 ng pcDNA5 FRT/TO to 2 µg pOG44. Afterwards, cells were selected in 100 µg/ml hygromycin B (H3274; Sigma-Aldrich). Cells were maintained in DMEM with 10% doxycycline-free FBS, 100 µg/ml hygromycin, and 15 µg/ml blasticidin at 37°C, 5% CO2. Expression of constructs close to endogenous levels was induced by incubation with 1 ng/ ml doxycyline for pcDNA5-V5-TurboID-L3 FRT/TO and pcDNA5-V5-TurboID-NES FRT/TO or 0.1 ng/ ml doxycycline for pcDNA5-V5-TurboID-TMEM192 FRT/TO for 24 hours. Proximity labelling was carried out as follows: Cells were incubated with 500 µM biotin (in DMSO) full medium for 15 min at 37°C, 5% CO2. The reaction was stopped by transferring plates on ice and medium was decanted. Cells were immediately spin-washed

three times with cold PBS and subsequently lysed in RIPA buffer supplemented with cOmplete™, Mini, EDTA-free protease-inhibitor cocktail (40694200; Roche) on ice. Cell lysates were transferred to low-binding microcentrifuge tubes (022431081; Eppendorf) and 1 mg protein in 1 ml total volume was incubated with 200 µl prewashed Streptavidin magnetic beads (88817; Pierce) at 4 °C overnight on a rotating wheel. The beads were washed three times with RIPA buffer and five times with detergent-free washing buffer (50 mM Tris-HCl, 50 mM NaCl, pH 7.4). Beads were kept on ice until further processing.

Sample preparation for mass spectrometry analysis

Beads were resuspended in 50 µL 1 M urea, 50 mM ammonium bicarbonate. Disulfide bonds were reduced with 2 µL of 250 mM dithiothreitol (DTT) for 30 min at room temperature before adding 2 µL of 500 mM iodoacetamide and incubating for 30 min at room temperature in the dark. Remaining iodoacetamide was quenched with 1 µL of 250 mM DTT for 10 min. Proteins were digested adding 300 ng trypsin (Trypsin Gold, Promega) followed by incubation at 37°C overnight. The digest was stopped by addition of trifluoroacetic acid (TFA) to a final concentration of 0.5 % and the supernatant was transferred to a fresh tube. The peptides were cleaned up according to the SP2 protocol by Waas et al. (2019).

Liquid chromatography - mass spectrometry analysis

Peptides were separated on an Ultimate 3000 RSLC nano-flow chromatography system (Thermo-Fisher Scientific), using a pre-column for sample loading (Acclaim PepMap C18, 2 cm × 0.1 mm, 5 µm, Thermo-Fisher Scientific), and a C18 analytical column (Acclaim PepMap C18, 50 cm × 0.75 mm, 2 µm, Thermo-Fisher Scientific), applying a segmented linear gradient from 2% to 35% over 120 min and finally 80% solvent B (80 % acetonitrile, 0.08 % formic acid;

solvent A 0.1 % formic acid) at a flow rate of 230 nL/min. The nano-LC was interfaced online via a nano-spray ion-source to a Q Exactive HF-X Orbitrap mass spectrometer (Thermo-Fisher Scientific). The mass spectrometer was operated in a data-dependent acquisition mode (DDA). Survey scans were obtained in a mass range of 375-1500 m/z, at a resolution of 120k at 200 m/z and an AGC target value of 3E6. The 8 most intense ions were selected with an isolation width of 1.6 m/z, at a target value of 1E5 with a max. IT of 250 ms, and fragmented in the HCD cell with 28% normalized collision energy. The spectra were recorded at a resolution of 30k. Peptides with a charge of +2 to +6 were included for fragmentation, the peptide match and the exclude isotopes features were enabled. Selected precursors were dynamically excluded from repeated sampling for 30 seconds.

Database search

MS raw data were analyzed using the MaxQuant software package (version 1.6.0.16, Tyanova et al., 2016) searching the Uniprot *Homo sapiens* reference proteome (www.uniprot.org), the sequences of the protein constructs as well as a database of common contaminants. The search was performed with full trypsin specificity and a maximum of two missed cleavages at a protein and peptide spectrum match false discovery rate of 1%. Carbamidomethylation of cysteine residues was set as fixed, oxidation of methionine and acetylation of the protein N-terminus as variable modifications. For label-free quantification the “match between runs” feature and the LFQ function were activated - all other parameters were left at default.

Proteomics data analysis

The output from MaxQuant was analyzed using amica (Didusch et al., 2022). Proteins from reverse database identifications, potential contaminant proteins and proteins only identified

by a modified peptide were removed. Proteins with at least 2 Razor + unique peptides, at least 3 MS/MS counts, and valid values in 3 replicates in at least one group were considered quantified. LFQ intensities of quantified proteins were log2-transformed and quantile normalized. Intensities with missing values were imputed from a normal distribution downshifted 1.8 standard deviations from the mean with a width of 0.3 standard deviations. Differential expression analysis was performed with DeqMS (version 1.10.0) (Zhu et al., 2020).

Over-Representation Analysis

Enriched proteins (log2 FC > 0 and padj ≤ 0.05) being both significantly enriched in the pairwise group comparisons L3/Cyto full medium and Lyso/Cyto full medium were used as an input for an over-representation analysis using gprofiler2 (version 0.2.1) (Raudvere et al., 2019) with the database Ensembl 104, Ensembl Genomes 51 (database built on 2021-05-07). The three branches of the Gene Ontology (GO:CC, GO:MF, GO:BP) (Ashburner et al., 2000; Carbon et al., 2021) were used as source databases for gprofiler2, excluding electronic GO annotations.

Network analysis

For the N-terminally tagged L3 bait (V5-T-L3), enriched proteins (log2 FC ≥ 1.49 and padj ≤ 0.05) were considered from all three conditions (pairwise group comparisons L3/Cyto in full medium, EBSS and EBSS+full medium). To remove unrelated nuclear proteins from this list of preys, proteins annotated with the term ‘nucleus’ (GO:0005634) that were not significantly enriched in the lyso control in at least one condition (log2 FC ≥ 1.49 and padj ≤ 0.05) were removed. The overlap of these preys in the three conditions was plotted (Figure S1J + K) using the eulerr package (version 6.1.1), and the pheatmap package (version 1.0.12) using colors

from ColorBrewer (Neuwirth, 2022). For the C-terminally tagged L3 bait (L3-T-V5), enriched proteins (log2 FC ≥ 1.49 and padj ≤ 0.05) were filtered in the same way to remove nuclear proteins.

Cytoscape (version 3.8.2) (Shannon et al., 2003) was used to create functional networks (Figure 1F, Figure S1D + I) of significant preys. Gene names from enriched proteins were loaded into the stringApp (version 1.7.1) (Doncheva et al., 2019) which returned a full STRING network (v11.5) (Szklarczyk et al., 2019) with a default confidence score cutoff of 0.4. Networks were visualized with the yFiles (v1.1.2) organic layout algorithm.

Quantification and statistical analysis

All image analysis was performed in Fiji distribution of ImageJ (Schindelin et al., 2012). Where indicated by white lines, the corresponding plots show the intensity profile of the respective channels along the length of the line. Profile plots were generated using the Plot Profile function in Fiji. Quantification of PLEKHG3 knockdown in immunofluorescence (IF) images: Single cells were segmented based on their combined PLEKHG3 and GFP channels by thresholding. From the resulting cell masks the integrated density (RawIntDens) was measured for both, GFP and PLEKHG3 channels after background subtraction. Superplots represent average values of 11 cells per condition from three technical replicates. Colocalization of Phalloidin with GFP and GFP-PLEKHG3 (Figure S3C) or LAMP1 with LAMTOR4 (Figure S3F) was performed on background subtracted images using the JACoP plugin (Bolte and Cordelières, 2006). Overlap of endogenous PLEKHG3 with LAMP1 and vice versa was analysed from background subtracted slide scanner images. High intensity and adjacent low

intensity regions were selected as ROIs in both channels and measured by RawIntDens. Similarly, the content of PLEKHG3 and lysosomes in elongated vs non-elongated protrusions was quantified by selecting them as ROIs and measuring RawIntDens from both channels. Colocalization analysis of FA structures with GFP, GFP-PLEKHG3, LAMTOR4 and LAMP1 was performed as follows: FA structures from single cells were defined as ROIs based on the Paxillin staining by segmentation which involved thresholding and particle size filtering. Control regions were defined by translocating the FA ROIs to adjacent regions. RawIntDens was measured for all channels of the respective experiment in all channels. Morphometric analysis was achieved by same FA segmentation as described above. Shape descriptor tools from Fiji (Area, Aspect ratio, Circularity) were applied on all FA ROIs. Morphometric analysis of cell shape was performed by segmenting single cells based on their GFP staining. Resulting cell masks were analysed for the above-mentioned shape descriptors. In live cell imaging analysis the shape descriptors were measured for all time points and then averaged over time. GFP and GFP-PLEKHG3 distribution in the cell was quantified by dividing the cells into peripheral, cytoplasmic and perinuclear regions. Perinuclear region was defined by enlarging the nucleus' outline based on DAPI staining and by 4 µm and subtraction of nucleus outline. Similarly, the cell outline was defined based the GFP channel which was subtracted by the outline shrunk by 4 µm. The cytosolic region was therefore defined as the whole cell of which peripheral and perinuclear regions were subtracted. For all regions RawIntDens was measured. Lysosomal distribution was performed based on an adapted Fiji macro from Filipek et al. (Filipek et al., 2017). In brief, the macro defines the center of mass of the nucleus based on DAPI staining and from there creates concentric annular ROIs with increasing radii. RawIntDens is measured in background subtracted LAMP1 channel. Quantification was performed on ≥ 14 cells (confocal images) or ≥ 50 cells (slide scanner images) per condition

from three biological replicates. Quantification of immunoblots was performed in Fiji. Two-tailed, paired Student's t tests were performed on experimental data from at least three independent experiments. Asterisks indicate the following significances: * = $p < 0.05$; ** = $p < 0.01$; *** = $p < 0.001$; **** = $p < 0.0001$.

Online supplemental material

Figure S1 shows validation of TurboID baits and bioinformatic analysis. Figure S2 shows validation of PLEKHG3 antibody and siRNA. Figure S3 shows effect of L3 KO on localization and function of GFP-PLEKHG3. Figure S4 shows that accumulation of peripheral lysosomes concentrates PLEKHG3 at PM. Movie S1-4 show L3 CTRL and KO cells expressing GFP or GFP-PLEKHG3. Movie S5 shows lysosomes moving into forming protrusions. Movies S6-11 show effect of changed lysosomal localization on protrusion formation and cell shape. Table S1 contains all hits identified by L3-T-V5 bait as displayed in Figure S1D. Table S2 contains all hits detected by V5-T-L3 as displayed in Figure S1I-K.

Acknowledgments

We are grateful M.E.G. de Araujo and T. Stasyk for helpful discussions, advice during the project and the gift of the HeLa cell line used in this study as well as a LAMTOR3 plasmid. We thank A. Ballabio and D. Medina for their support at TIGEM. We are grateful to C. Guardia who kindly provided us with a KIF1A plasmid, the MPL FACS facility and the MPL BioOptics facility, especially I. Fischer and T. Peterbauer for assistance with imaging and macro writing. We thank the MPL Mass Spectrometry Facility which performed the proteomics analysis with assistance of N. Hartl and D. Anrather using the VBCF instrument pool. We thank S. Martens for advice during the project.

This work was supported by the Austrian Science Fund W-1220 “Signaling mechanisms in cellular homeostasis” (to M. Baccarini) and by funds of the University of Vienna (to M. Baccarini). G. Vucak is a recipient of a DOC-fellowship of the Austrian Academy of Sciences at the Max Perutz Labs. L.A. Huber is funded by the Austrian Science Fund P-32608.

Author contributions: R. Ettelt performed most of the experiments. G. Vucak contributed the L3-T-V5 screen data and immunoblots. S. Didusch performed the bioinformatic analysis of MS data and helped in microscopic data analysis. B. Riemelmoser performed selected cell biology and biochemistry experiments. Karin Ehrenreiter helped with the generation of stable cell lines. M. Hartl performed the mass spectrometry. M. Baccarini, R. Ettelt and L. A. Huber wrote the manuscript. The whole project was supervised by M. Baccarini.

COMPETING INTERESTS

The authors declare no competing financial interests.

References

Andrews, N.W. 2000. Regulated secretion of conventional lysosomes. *Trends Cell Biol*. 10:316–321. doi:10.1016/S0962-8924(00)01794-3.

de Araujo, M.E.G., G. Liebscher, M.W. Hess, and L.A. Huber. 2020. Lysosomal size matters. *Traffic*. 21:60–75. doi:10.1111/tra.12714.

de Araujo, M.E.G., A. Naschberger, B.G. Fürnrohr, T. Stasyk, T. Dunzendorfer-Matt, S. Lechner, S. Welti, L. Kremser, G. Shivalingaiah, M. Offterdinger, H.H. Lindner, L.A. Huber, and K. Scheffzek. 2017. Crystal structure of the human lysosomal mTORC1 scaffold complex and its impact on signaling. *Science (1979)*. 358:377–381. doi:10.1126/science.aao1583.

de Araújo, M.E.G., T. Stasyk, N. Taub, H.L. Ebner, B. Fürst, P. Filipek, S.R. Weys, M.W. Hess, H. Lindner, L. Kremser, and L.A. Huber. 2013. Stability of the endosomal scaffold protein lAMTOR3 depends on heterodimer assembly and proteasomal degradation. *Journal of Biological Chemistry*. 288:18228–18242. doi:10.1074/jbc.M112.349480.

Ashburner, M., C.A. Ball, J.A. Blake, D. Botstein, H. Butler, J.M. Cherry, A.P. Davis, K. Dolinski, S.S. Dwight, J.T. Eppig, M.A. Harris, D.P. Hill, L. Issel-Tarver, A. Kasarskis, S. Lewis, J.C. Matese, J.E. Richardson, M. Ringwald, G.M. Rubin, and G. Sherlock. 2000. Gene Ontology: tool for the unification of biology. *Nature Genetics 2000 25:1*. 25:25–29. doi:10.1038/75556.

Bagci, H., N. Sriskandarajah, A. Robert, J. Boulais, I.E. Elkholi, V. Tran, Z.Y. Lin, M.P. Thibault, N. Dubé, D. Faubert, D.R. Hipfner, A.C. Gingras, and J.F. Côté. 2020. Mapping the proximity interaction network of the Rho-family GTPases reveals signalling pathways and regulatory mechanisms. *Nat Cell Biol*. 22:120–134. doi:10.1038/s41556-019-0438-7.

Bagshaw, R.D., D.J. Mahuran, and J.W. Callahan. 2005. A proteomic analysis of lysosomal integral membrane proteins reveals the diverse composition of the organelle. *Molecular and Cellular Proteomics*. 4:133–143. doi:10.1074/mcp.M400128-MCP200.

Bagshaw, R.D., S.H. Pasternak, D.J. Mahuran, and J.W. Callahan. 2003. Nicastrin is a resident lysosomal membrane protein. *Biochem Biophys Res Commun*. 300:615–618. doi:10.1016/S0006-291X(02)02865-6.

Ballabio, A., and J.S. Bonifacino. 2020. Lysosomes as dynamic regulators of cell and organismal homeostasis. *Nat Rev Mol Cell Biol*. 21:101–118. doi:10.1038/s41580-019-0185-4.

Bolte, S., and F.P. Cordelières. 2006. A guided tour into subcellular colocalization analysis in light microscopy. *J Microsc*. 224:213–232. doi:10.1111/J.1365-2818.2006.01706.X.

Buratta, S., B. Tancini, K. Sagini, F. Delo, E. Chiaradia, L. Urbanelli, and C. Emiliani. 2020. Lysosomal Exocytosis, Exosome Release and Secretory Autophagy: The Autophagic- and Endo-Lysosomal Systems Go Extracellular. *International Journal of Molecular Sciences 2020, Vol. 21, Page 2576*. 21:2576. doi:10.3390/IJMS21072576.

Burridge, K., and C.K. Burridge. 2017. Focal adhesions: a personal perspective on a half century of progress. *FEBS J*. 284:3355–3361. doi:10.1111/FEBS.14195.

Cabukusta, B., and J. Neefjes. 2018. Mechanisms of lysosomal positioning and movement. *Traffic*. 19:761–769. doi:10.1111/tra.12587.

Carbon, S., E. Douglass, B.M. Good, D.R. Unni, N.L. Harris, C.J. Mungall, S. Basu, R.L. Chisholm, R.J. Dodson, E. Hartline, P. Fey, P.D. Thomas, L.P. Albou, D. Ebert, M.J. Kesling, H. Mi, A. Muruganujan, X. Huang, T. Mushayahama, S.A. LaBonte, D.A. Siegele,

G. Antonazzo, H. Attrill, N.H. Brown, P. Garapati, S.J. Marygold, V. Trovisco, G. dos Santos, K. Falls, C. Tabone, P. Zhou, J.L. Goodman, V.B. Strelets, J. Thurmond, P. Garmiri, R. Ishtiaq, M. Rodríguez-López, M.L. Acencio, M. Kuiper, A. Lægreid, C. Logie, R.C. Lovering, B. Kramarz, S.C.C. Saverimuttu, S.M. Pinheiro, H. Gunn, R. Su, K.E. Thurlow, M. Chibucos, M. Giglio, S. Nadendla, J. Munro, R. Jackson, M.J. Duesbury, N. Del-Toro, B.H.M. Meldal, K. Paneerselvam, L. Perfetto, P. Porras, S. Orchard, A. Shrivastava, H.Y. Chang, R.D. Finn, A.L. Mitchell, N.D. Rawlings, L. Richardson, A. Sangrador-Vegas, J.A. Blake, K.R. Christie, M.E. Dolan, H.J. Drabkin, D.P. Hill, L. Ni, D.M. Sitnikov, M.A. Harris, S.G. Oliver, K. Rutherford, V. Wood, J. Hayles, J. Bähler, E.R. Bolton, J.L. de Pons, M.R. Dwinell, G.T. Hayman, M.L. Kaldunski, A.E. Kwitek, S.J.F. Laulederkind, C. Plasterer, M.A. Tutaj, M. Vedi, S.J. Wang, P. D'Eustachio, L. Matthews, J.P. Balhoff, S.A. Aleksander, M.J. Alexander, J.M. Cherry, S.R. Engel, et al. 2021. The Gene Ontology resource: enriching a GOld mine. *Nucleic Acids Res*. 49:D325–D334. doi:10.1093/NAR/GKAA1113.

Caviston, J.P., A.L. Zajac, M. Tokito, and E.L.F. Holzbaur. 2011. Huntingtin coordinates the dynein-mediated dynamic positioning of endosomes and lysosomes. *Mol Biol Cell*. 22:478–492. doi:10.1091/MBC.E10-03-0233/ASSET/IMAGES/LARGE/478FIG9.JPEG.

Chapel, A., S. Kieffer-Jaquinod, C. Sagné, Q. Verdon, C. Ivaldi, M. Mellal, J. Thirion, M. Jadot, C. Bruley, J. Garin, B. Gasnier, and A. Journet. 2013. An extended proteome map of the lysosomal membrane reveals novel potential transporters. *Molecular and Cellular Proteomics*. 12:1572–1588. doi:10.1074/mcp.M112.021980.

Colaço, A., and M. Jäättelä. 2017. Ragulator-a multifaceted regulator of lysosomal signaling and trafficking. *J Cell Biol*. 216:3895–3898. doi:10.1083/jcb.201710039 PM - 29138253 M4 - Citavi.

Condeelis, J., and R.H. Singer. 2005. How and why does β-actin mRNA target? *Biol Cell*. 97:97–110. doi:10.1042/BC20040063.

Cordonnier, M.N., D. Dauzonne, D. Louvard, and E. Coudrier. 2001. Actin filaments and myosin I alpha cooperate with microtubules for the movement of lysosomes. *Mol Biol Cell*. 12:4013–4029. doi:10.1091/MBC.12.12.4013/ASSET/IMAGES/LARGE/MK1211695012.JPEG.

Didusch, S., M. Madern, M. Hartl, and M. Baccarini. 2022. amica: an interactive and user-friendly web-platform for the analysis of proteomics data. *BMC Genomics 2022 23:1*. 23:1–9. doi:10.1186/S12864-022-09058-7.

Doncheva, N.T., J.H. Morris, J. Gorodkin, and L.J. Jensen. 2019. Cytoscape StringApp: Network Analysis and Visualization of Proteomics Data. *J Proteome Res*. 18:623–632. doi:10.1021/ACS.JPROTEOME.8B00702/SUPPL_FILE/PR8B00702_SI_002.XLSX.

Dozynkiewicz, M.A., N.B. Jamieson, I. MacPherson, J. Grindlay, P.V.E. vandenBerghe, A. vonThun, J.P. Morton, C. Gourley, P. Timpson, C. Nixon, C.J. McKay, R. Carter, D. Strachan, K. Anderson, O.J. Sansom, P.T. Caswell, and J.C. Norman. 2012. Rab25 and CLIC3 Collaborate to Promote Integrin Recycling from Late Endosomes/Lysosomes and Drive Cancer Progression. *Dev Cell*. 22:131–145. doi:10.1016/j.devcel.2011.11.008.

Dykes, S.S., A.L. Gray, D.T. Coleman, M. Saxena, C.A. Stephens, J.L. Carroll, K. Pruitt, and J.A. Cardelli. 2016. The Arf-like GTPase Arl8b is essential for three-dimensional invasive growth of prostate cancer in vitro and xenograft formation and growth in vivo. *Oncotarget*. 7:31037–31052. doi:10.18632/oncotarget.8832.

Egri, S.B., C. Ouch, H.T. Chou, Z. Yu, K. Song, C. Xu, and K. Shen. 2022. Cryo-EM structures of the human GATOR1-Rag-Ragulator complex reveal a spatial-constraint regulated GAP mechanism. *Mol Cell*. 82:1836-1849.e5. doi:10.1016/j.molcel.2022.03.002.

Encarnação, M., L. Espada, C. Escrevente, D. Mateus, J. Ramalho, X. Michelet, I. Santarino, V.W. Hsu, M.B. Brenner, D.C. Barral, and O. v. Vieira. 2016. A Rab3a-dependent complex essential for lysosome positioning and plasma membrane repair. *Journal of Cell Biology*. 213:631–640. doi:10.1083/JCB.201511093.

Filipek, P.A., M.E.G. Araujo, G.F. Vogel, C.H. Smet, D. Eberharter, M. Rebsamen, E.L. Rudashevskaya, L. Kremser, T. Yordanov, P. Tschaikner, B.G. Fürnrohr, S. Lechner, T. Dunzendorfer-Matt, K. Scheffzek, K.L. Bennett, G. Superti-Furga, H.H. Lindner, T. Stasyk, and L.A. Huber. 2017. LAMTOR/Ragulator is a negative regulator of Arl8b- and BORC-dependent late endosomal positioning. *J Cell Biol*. 216:4199–4215. doi:10.1083/jcb.201703061 PM - 28993467 M4 - Citavi.

Garcin, C., and A. Straube. 2019. Microtubules in cell migration. *Essays Biochem*. 63:509–520. doi:10.1042/EBC20190016.

Gardel, M.L., I.C. Schneider, Y. Aratyn-Schaus, and C.M. Waterman. 2010. Mechanical Integration of Actin and Adhesion Dynamics in Cell Migration. *https://doi.org/10.1146/annurev.cellbio.011209.122036*. 26:315–333. doi:10.1146/ANNUREV.CELLBIO.011209.122036.

Go, C.D., J.D.R. Knight, A. Rajasekharan, B. Rathod, G.G. Hesketh, K.T. Abe, J.Y. Youn, P. Samavarchi-Tehrani, H. Zhang, L.Y. Zhu, E. Popiel, J.P. Lambert, É. Coyaud, S.W.T. Cheung, D. Rajendran, C.J. Wong, H. Antonicka, L. Pelletier, A.F. Palazzo, E.A. Shoubridge, B. Raught, and A.C. Gingras. 2021. A proximity-dependent biotinylation map of a human cell. *Nature 2021 595:7865*. 595:120–124. doi:10.1038/s41586-021-03592-2.

Guardia, C.M., G.G. Farías, R. Jia, J. Pu, and J.S. Bonifacino. 2016. BORC Functions Upstream of Kinesins 1 and 3 to Coordinate Regional Movement of Lysosomes along Different Microtubule Tracks. *Cell Rep*. 17:1950–1961. doi:10.1016/j.celrep.2016.10.062.

Hong, Z., N.M. Pedersen, L. Wang, M.L. Torgersen, H. Stenmark, and C. Raiborg. 2017. PtdIns3P controls mTORC1 signaling through lysosomal positioning. *Journal of Cell Biology*. 216:4217–4233. doi:10.1083/JCB.201611073.

Johnson, D.E., P. Ostrowski, V. Jaumouillé, and S. Grinstein. 2016. The position of lysosomes within the cell determines their luminal pH. *Journal of Cell Biology*. 212:677–692. doi:10.1083/jcb.201507112.

Johnsson, A.K., and R. Karlsson. 2010. Microtubule-dependent localization of profilin I mRNA to actin polymerization sites in serum-stimulated cells. *Eur J Cell Biol*. 89:394–401. doi:10.1016/J.EJCB.2009.10.020.

Keren-Kaplan, T., A. Sarić, S. Ghosh, C.D. Williamson, R. Jia, Y. Li, and J.S. Bonifacino. 2022. RUFY3 and RUFY4 are ARL8 effectors that promote coupling of endolysosomes to dynein-dynactin. *Nature Communications 2022 13:1*. 13:1–22. doi:10.1038/s41467-022-28952-y.

Korolchuk, V.I., S. Saiki, M. Lichtenberg, F.H. Siddiqi, E.A. Roberts, S. Imarisio, L. Jahreiss, S. Sarkar, M. Futter, F.M. Menzies, C.J. O'Kane, V. Deretic, and D.C. Rubinsztein. 2011. Lysosomal positioning coordinates cellular nutrient responses. *Nat Cell Biol*. 13:453–462. doi:10.1038/ncb2204.

Kumar, G., P. Chawla, N. Dhiman, S. Chadha, S. Sharma, K. Sethi, M. Sharma, and A. Tuli. 2022. RUFY3 links Arl8b and JIP4-Dynein complex to regulate lysosome size and

positioning. *Nature Communications 2022 13:1*. 13:1–21. doi:10.1038/s41467-022-29077-y.

Lawson, M.A., and F.R. Maxfield. 1995. Ca2+- and calcineurin-dependent recycling of an integrin to the front of migrating neutrophils. *Nature 1995 377:6544*. 377:75–79. doi:10.1038/377075a0.

Liao, Y.C., M.S. Fernandopulle, G. Wang, H. Choi, L. Hao, C.M. Drerup, R. Patel, S. Qamar, J. Nixon-Abell, Y. Shen, W. Meadows, M. Vendruscolo, T.P.J. Knowles, M. Nelson, M.A. Czekalska, G. Musteikyte, M.A. Gachechiladze, C.A. Stephens, H.A. Pasolli, L.R. Forrest, P. St George-Hyslop, J. Lippincott-Schwartz, and M.E. Ward. 2019. RNA Granules Hitchhike on Lysosomes for Long-Distance Transport, Using Annexin A11 as a Molecular Tether. *Cell*. 179:147-164.e20. doi:10.1016/J.CELL.2019.08.050.

Liu, X., K. Salokas, F. Tamene, Y. Jiu, R.G. Weldatsadik, T. Öhman, and M. Varjosalo. 2018. An AP-MS- and BioID-compatible MAC-tag enables comprehensive mapping of protein interactions and subcellular localizations. *Nature Communications 2018 9:1*. 9:1–16. doi:10.1038/s41467-018-03523-2.

Marwaha, R., S. Rawal, P. Khuntia, M. Jaiswal, and T. Das. 2022. Mechanosensitive dynamics of lysosomes regulates the emergence of leader cells during collective cell migration. *bioRxiv*. 2022.08.03.502740. doi:10.1101/2022.08.03.502740.

Medina, D.L., A. Fraldi, V. Bouche, F. Annunziata, G. Mansueto, C. Spampanato, C. Puri, A. Pignata, J.A. Martina, M. Sardiello, M. Palmieri, R. Polishchuk, R. Puertollano, and A. Ballabio. 2011. Transcriptional activation of lysosomal exocytosis promotes cellular clearance. *Dev Cell*. 21:421–430. doi:10.1016/j.devcel.2011.07.016.

Mohamed, M.M., and B.F. Sloane. 2006. multifunctional enzymes in cancer. *Nature Reviews Cancer 2006 6:10*. 6:764–775. doi:10.1038/nrc1949.

Nada, S., A. Hondo, A. Kasai, M. Koike, K. Saito, Y. Uchiyama, and M. Okada. 2009. The novel lipid raft adaptor p18 controls endosome dynamics by anchoring the MEK-ERK pathway to late endosomes. *EMBO Journal*. 28:477–489. doi:10.1038/emboj.2008.308.

Neuwirth, E. 2022. ColorBrewer Palettes [R package RColorBrewer version 1.1-3].

Nguyen, T.L., J. Schneppenheim, S. Rudnik, R. Lüllmann-Rauch, C. Bernreuther, I. Hermans-Borgmeyer, M. Glatzel, P. Saftig, and B. Schröder. 2017. Functional characterization of the lysosomal membrane protein TMEM192 in mice. *Oncotarget*. 8:43635–43652. doi:10.18632/oncotarget.17514.

Nguyen, T.T.T., W.S. Park, B.O. Park, C.Y. Kim, Y. Oh, J.M. Kim, H. Choi, T. Kyung, C.H. Kim, G. Lee, K.M. Hahn, T. Meyer, and W. do Heo. 2016. PLEKHG3 enhances polarized cell migration by activating actin filaments at the cell front. *Proc Natl Acad Sci U S A*. 113:10091–10096. doi:10.1073/pnas.1604720113.

Pu, J., C.M. Guardia, T. Keren-Kaplan, and J.S. Bonifacino. 2016. Mechanisms and functions of lysosome positioning. *J Cell Sci*. 129:4329–4339. doi:10.1242/jcs.196287.

Pu, J., T. Keren-Kaplan, and J.S. Bonifacino. 2017. A Ragulator-BORC interaction controls lysosome positioning in response to amino acid availability. *Journal of Cell Biology*. 216:4183–4197. doi:10.1083/jcb.201703094.

Rabanal-Ruiz, Y., A. Byron, A. Wirth, R. Madsen, L. Sedlackova, G. Hewitt, G. Nelson, J. Stingele, J.C. Wills, T. Zhang, A. Zeug, R. Fässler, B. Vanhaesebroeck, O.D.K. Maddocks, E. Ponimaskin, B. Carroll, and V.I. Korolchuk. 2021. mTORC1 activity is supported by spatial association with focal adhesions. *Journal of Cell Biology*. 220. doi:10.1083/JCB.202004010.

Ran, F.A., P.D. Hsu, J. Wright, V. Agarwala, D.A. Scott, and F. Zhang. 2013. Genome engineering using the CRISPR-Cas9 system. *Nature Protocols 2013 8:11*. 8:2281–2308. doi:10.1038/nprot.2013.143.

Raudvere, U., L. Kolberg, I. Kuzmin, T. Arak, P. Adler, H. Peterson, and J. Vilo. 2019. g:Profiler: a web server for functional enrichment analysis and conversions of gene lists (2019 update). *Nucleic Acids Res*. 47:W191–W198. doi:10.1093/NAR/GKZ369.

Rodríguez, A., P. Webster, J. Ortego, and N.W. Andrews. 1997. Lysosomes Behave as Ca2+-regulated Exocytic Vesicles in Fibroblasts and Epithelial Cells. *Journal of Cell Biology*. 137:93–104. doi:10.1083/JCB.137.1.93.

Rogala, K.B., X. Gu, J.F. Kedir, M. Abu-Remaileh, L.F. Bianchi1, A.M.S. Bottino1, R. Dueholm1, A. Niehaus1, D. Overwijn1, A.C. Priso Fils1, S.X. Zhou1, D. Leary, N.N. Laqtom1, E.J. Brignole, and D.M. Sabatini. 2019. Structural basis for the docking of mTORC1 on the lysosomal surface. *Science (1979)*. 366:468–475. doi:10.1126/science.aay0166.

Sancak, Y., L. Bar-Peled, R. Zoncu, A.L. Markhard, S. Nada, and D.M. Sabatini. 2010. Ragulator-rag complex targets mTORC1 to the lysosomal surface and is necessary for its activation by amino acids. *Cell*. 141:290–303. doi:10.1016/j.cell.2010.02.024.

Schiefermeier, N., J.M. Scheffler, M.E.G. de Araujo, T. Stasyk, T. Yordanov, H.L. Ebner, M. Offterdinger, S. Munck, M.W. Hess, S.A. Wickström, A. Lange, W. Wunderlich, R. Fässler, D. Teis, and L.A. Huber. 2014. The late endosomal p14-MP1 (LAMTOR2/3) complex regulates focal adhesion dynamics during cell migration. *Journal of Cell Biology*. 205:525–540. doi:10.1083/jcb.201310043.

Schindelin, J., I. Arganda-Carreras, E. Frise, V. Kaynig, M. Longair, T. Pietzsch, S. Preibisch, C. Rueden, S. Saalfeld, B. Schmid, J.Y. Tinevez, D.J. White, V. Hartenstein, K. Eliceiri, P. Tomancak, and A. Cardona. 2012. Fiji: an open-source platform for biological-image analysis. *Nature Methods 2012 9:7*. 9:676–682. doi:10.1038/nmeth.2019.

Schröder, B., C. Wrocklage, C. Pan, R. Jäger, B. Kösters, H. Schäfer, H.P. Elsässer, M. Mann, and A. Hasilik. 2007. Integral and Associated Lysosomal Membrane Proteins. *Traffic*. 8:1676–1686. doi:10.1111/J.1600-0854.2007.00643.X.

Shannon, P., A. Markiel, O. Ozier, N.S. Baliga, J.T. Wang, D. Ramage, N. Amin, B. Schwikowski, and T. Ideker. 2003. Cytoscape: A Software Environment for Integrated Models of Biomolecular Interaction Networks. *Genome Res*. 13:2498–2504. doi:10.1101/GR.1239303.

Steffan, J.J., B.C. Williams, T. Welbourne, and J.A. Cardelli. 2010. HGF-induced invasion by prostate tumor cells requires anterograde lysosome trafficking and activity of Na+-H+ exchangers. *J Cell Sci*. 123:1151–1159. doi:10.1242/JCS.063644.

Szklarczyk, D., A.L. Gable, D. Lyon, A. Junge, S. Wyder, J. Huerta-Cepas, M. Simonovic, N.T. Doncheva, J.H. Morris, P. Bork, L.J. Jensen, and C. von Mering. 2019. STRING v11: protein–protein association networks with increased coverage, supporting functional discovery in genome-wide experimental datasets. *Nucleic Acids Res*. 47:D607–D613. doi:10.1093/NAR/GKY1131.

Tan, J.X., and T. Finkel. 2022. A phosphoinositide signalling pathway mediates rapid lysosomal repair. *Nature 2022 609:7928*. 609:815–821. doi:10.1038/s41586-022-05164-4.

Teis, D., W. Wunderlich, and L.A. Huber. 2002. Localization of the MP1-MAPK scaffold complex to endosomes is mediated by p14 and required for signal transduction. *Dev Cell*. 3:803–814. doi:10.1016/S1534-5807(02)00364-7.

della Valle, M.C., D.E. Sleat, H. Zheng, D.F. Moore, M. Jadot, and P. Lobel. 2011. Classification of subcellular location by comparative proteomic analysis of native and density-shifted lysosomes. *Molecular and Cellular Proteomics*. 10:M110.006403. doi:10.1074/mcp.M110.006403.

Vogel, G.F., H.L. Ebner, M.E.G. de Araujo, T. Schmiedinger, O. Eiter, H. Pircher, K. Gutleben, B. Witting, D. Teis, L.A. Huber, and M.W. Hess. 2015. Ultrastructural Morphometry Points to a New Role for LAMTOR2 in Regulating the Endo/Lysosomal System. *Traffic*. 16:617–634. doi:10.1111/tra.12271.

Zhang, C.S., B. Jiang, M. Li, M. Zhu, Y. Peng, Y.L. Zhang, Y.Q. Wu, T.Y. Li, Y. Liang, Z. Lu, G. Lian, Q. Liu, H. Guo, Z. Yin, Z. Ye, J. Han, J.W. Wu, H. Yin, S.Y. Lin, and S.C. Lin. 2014. The lysosomal v-ATPase-ragulator complex is a common activator for AMPK and mTORC1, acting as a switch between catabolism and anabolism. *Cell Metab*. 20:526–540. doi:10.1016/j.cmet.2014.06.014.

Zhu, Y., L.M. Orre, Y.Z. Tran, G. Mermelekas, H.J. Johansson, A. Malyutina, S. Anders, and J. Lehtiö. 2020. DEqMS: A method for accurate variance estimation in differential protein expression analysis. *Molecular and Cellular Proteomics*. 19:1047–1057. doi:10.1074/mcp.TIR119.001646.